Yogodzinski, G. M., Bizimis, M., Hickey-Vargas, R., McCarthy, A., Hocking, B. D., Savov, I. P., Ishizuka, O., & Arculus, R. (2018). Implications of Eocene-age Philippine Sea and forearc basalts for initiation and early history of the Izu-Bonin-Mariana arc. *Geochimica et Cosmochimica Acta*, *228*, 136-156. https://doi.org/10.1016/j.gca.2018.02.047

Available online at www.sciencedirect.com

ScienceDirect

Geochimica et Cosmochimica Acta 228 (2018) 136–156

Geochimica et Cosmochimica Acta

www.elsevier.com/locate/gca

Implications of Eocene-age Philippine Sea and forearc basalts for initiation and early history of the Izu-Bonin-Mariana arc

Gene M. Yogodzinski [a,*], Michael Bizimis [a], Rosemary Hickey-Vargas [b], Anders McCarthy [c,1], Benjamin D. Hocking [a], Ivan P. Savov [d], Osamu Ishizuka [e,f], Richard Arculus [g]

[a] School of Earth, Ocean, and Environment, University of South Carolina, 701 Sumter St., EWSC617, Columbia, SC 29208-3402 USA
[b] Department of Earth and Environment, AHC5-394, Florida International University, Miami, FL 33199, USA
[c] Institute of Earth Sciences, University of Lausanne, Geopolis, Lausanne 1015, Switzerland
[d] School of Earth and Environment, Institute of Geophysics and Tectonics, University of Leeds, Leeds LS2 9JT, UK
[e] Geological Survey of Japan/AIST, Central 7 1-1-1, Higashi, Tsukuba, Ibaraki 305-8567, Japan
[f] Research and Development Center for Ocean Drilling Science, Japan Agency for Marine-Earth Science and Technology, 2-15 Natsushima-cho, Yokosuka 237-0061, Japan
[g] Research School of Earth Sciences, Australian National University, Canberra, ACT 2601, Australia

Received 28 July 2017; accepted in revised form 27 February 2018; available online 8 March 2018

Abstract

Whole-rock isotope ratio (Hf, Nd, Pb, Sr) and trace element data for basement rocks at ocean drilling Sites U1438, 1201 and 447 immediately west of the KPR (Kyushu-Palau Ridge) are compared to those of FAB (forearc basalts) previously interpreted to be the initial products of IBM subduction volcanism. West-of-KPR basement basalts (drill sites U1438, 1201, 447) and FAB occupy the same Hf-Nd and Pb-Pb isotopic space and share distinctive source characteristics with ε_{Hf} mostly > 16.5 and up to $\varepsilon_{Hf} = 19.8$, which is more radiogenic than most Indian mid-ocean ridge basalts (MORB). Lead isotopic ratios are depleted, with $^{206}Pb/^{204}Pb = 17.8–18.8$ accompanying relatively high $^{208}Pb/^{204}Pb$, indicating an Indian-MORB source unlike that of West Philippine Basin plume basalts. Some Sr isotopes show affects of seawater alteration, but samples with $^{87}Sr/^{86}Sr < 0.7034$ and $\varepsilon_{Nd} > 8.0$ appear to preserve magmatic compositions and also indicate a common source for west-of-KPR basement and FAB. Trace element ratios resistant to seawater alteration (La/Yb, Lu/Hf, Zr/Nb, Sm/Nd) in west-of-KPR basement are generally more depleted than normal MORB and so also appear similar to FAB. At Site U1438, only andesite sills intruding sedimentary rocks overlying the basement have subduction-influenced geochemical characteristics ($\varepsilon_{Nd} \sim 6.6$, $\varepsilon_{Hf} \sim 13.8$, La/Yb > 2.5, Nd/Hf ~ 9). The key characteristic that unites drill site basement rocks west of KPR and FAB is the nature of their source, which is more depleted in lithophile trace elements than average MORB but with Hf, Nd, and Pb isotope ratios that are common in MORB. The lithophile element-depleted nature of FAB has been linked to initiation of IBM subduction in the Eocene, but Sm-Nd model ages and errorchron relationships in Site U1438 basement indicate that the depleted

* Corresponding author.
E-mail addresses: gyogodzin@geol.sc.edu (G.M. Yogodzinski), mbizimis@geol.sc.edu (M. Bizimis), hickey@fiu.edu (R. Hickey-Vargas), anders.mccarthy@unil.ch (A. McCarthy), bdhocking13@gmail.com (B.D. Hocking), i.savov@leeds.ac.uk (I.P. Savov), o-ishizuka@aist.go.jp (O. Ishizuka), richard.arculus@anu.edu.au (R. Arculus).
[1] Present address: School of Earth Sciences, University of Bristol, Wills Memorial Building, Queens Road, Clifton BS8 1RJ, UK.

https://doi.org/10.1016/j.gca.2018.02.047

character of the rocks is a regional characteristic that was produced well prior to the time of subduction initiation and persists today in the source of modern IBM arc volcanic rocks with Sm/Nd > 0.34 and $\varepsilon_{Nd} \sim 9.0$.

1. INTRODUCTION

In 2014, Expeditions 351 and 352 of the International Ocean Discovery Program (IODP) were conducted in the western Pacific south of Japan. The goal of these expeditions was to achieve an improved understanding of geologic processes leading up to and following initiation of the Izu-Bonin-Mariana (IBM) subduction system. For Expedition 351, the primary goal was to characterize the oceanic lithosphere upon which the IBM arc was constructed and to interpret the sedimentary record of events that accompanied the onset of subduction and early history of the arc (Arculus et al., 2013).

Drilling on Expedition 351 was at Site U1438, at 27.5° N and ~50 km southwest of the nearest volcanic edifices of the Kyushu-Palau Ridge (KPR, Fig. 1). The site lies within a triangular complex of ridges and seamounts north of the West Philippine Basin and is bounded by the KPR and Ryuku Trench (Fig. 1). Karig (1975) inferred a Cretaceous or Paleocene age for these ridges and their bounding basins from geological and heat-flow observations. Findings of most subsequent work appeared consistent with these conclusions (Ozima et al., 1983; Hickey-Vargas, 1998; Deschamps and Lallemand, 2002; Hickey-Vargas, 2005; Ishizuka et al., 2013; Lallemand, 2016), but biostratigraphic and heat-flow data acquired from drilling in 2014 showed that oceanic lithosphere at Site U1438 was likely formed in the early Eocene (Arculus et al., 2015b). Subsequent radioisotopic dating has shown that basement rocks at Site U1438 are ~49 Ma (Ishizuka et al., 2018). These results imply that Site U1438 basement provides an opportunity not to study the pre-subduction foundation of the IBM arc, but instead, to characterize tectono-magmatic events close in time to initiation of IBM subduction, which is currently inferred to have occurred at ~52 Ma (Ishizuka et al., 2011).

This paper reports new Hf, Nd, Sr, and Pb isotopic data for basement basalts recovered by drilling at Site U1438 during IODP Expedition 351. We also report new trace element and Hf-Nd isotopic data for basaltic basement at drill sites 1201 and 447 and for basalts collected by submersible in the modern forearc at 32° N (samples from DeBari et al., 1999). We use these data to document regional, geochemical patterns of volcanism in the West Philippine Basin in the Eocene. In a companion paper (Hickey-Vargas et al., 2018), we use major and trace element data to establish a stratigraphic succession for Site U1438 basement, and to interpret the origins of the site. The over-arching goal of the combined papers is evaluate the idea that basalts with FAB geochemistry were produced not only at the front (forearc) of the proto IBM arc (Reagan et al., 2010; Ishizuka et al., 2011), but also on the backarc side (west of the KPR) in extensional settings created by the foundering of a dense lithospheric plate at the time of IBM subduction initiation (Arculus et al., 2015b).

2. BACKGROUND

A central conclusion from most studies of the 1980s and 1990s was that the first volcanic products of IBM subduction were boninites and boninite-related andesites and dacites (Meijer, 1980; Hickey and Frey, 1982; Cameron et al., 1983; Bloomer and Hawkins, 1987; Pearce et al., 1992; Stern and Bloomer, 1992). These studies were based on samples from forearc islands, dredging of the inner trench wall, and from drilling in the forearc at DSDP Sites 458 and 459 and ODP Site 786 (Fig. 1). DeBari et al. (1999) subsequently identified a layer of basalt by submersible observations on the inner trench wall of the modern arc at ~32°N and at depths ~3000 m below the boninites drilled at Site 786 (Fig. 1). The distinctive compositions of these basalts (more depleted than normal MORB) are similar to West Philippine Basin basalts at DSDP Site 447 (Fig. 1) and unlike the basalts produced by backarc spreading east of the KPR. This led DeBari et al. (1999) to interpret the trench wall samples as fragments of West Philippine Basin crust, which were the foundation upon which the IBM arc was built, and which were trapped in the forearc at 25 Ma following the rifting of the proto IBM arc and initial opening of the Shikoku and Parece-Vela basins. Thus, depleted basalts exposed on the inner trench wall were initially interpreted to record volcanic activity prior to the onset of IBM subduction, which was still assumed to be marked by the overlying boninites (DeBari et al., 1999).

More recent submersible dives at ~12°N, and ~28°N (Fig. 1) also identified basalts beneath boninites on the inner trench wall (Reagan et al., 2010; Ishizuka et al., 2011). These studies again noted the depleted character of the basalts and interpreted them as a transitional geochemical type more depleted in lithophile trace elements than MORB but less depleted than boninites. The presence of geochemically similar basalts underlying boninites in three areas widely separated along-strike (submersible dive locations shown on Fig. 1) suggested a common geological and geochemical succession for the whole IBM arc. This led to the interpretation of these basalts not as a stranded sliver of West Philippine Basin crust (DeBari et al., 1999) but as the earliest products of IBM volcanism (Reagan et al., 2010; Ishizuka et al., 2011).

Reagan et al. (2010) termed the early basalts FAB (forearc basalts) and described them as tholeiites with trace element patterns more depleted than average MORB, and with some signatures reflecting subduction influence. They interpreted FAB to be the initial products of mantle wedge melting, formed by upwelling around the leading edge of a

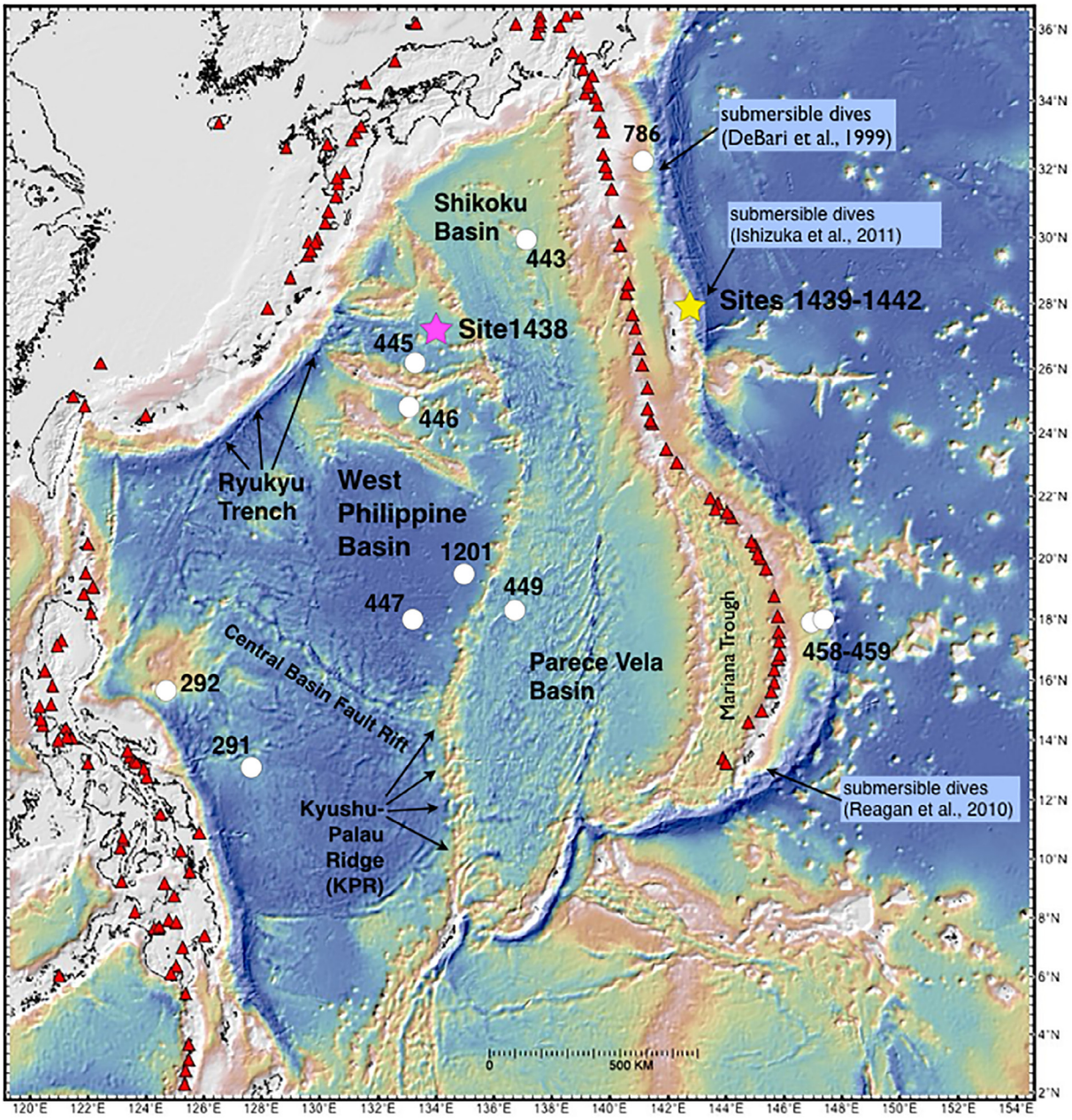

Fig. 1. Map of the western Pacific region, showing the West Philippine Basin and Izu-Bonin-Mariana (IBM) subduction system and other locations mentioned in the text. Pink and yellow stars mark the locations of IODP Expeditions 351 (Site U1438) and 352 (Sites 1439-1442). White dots are locations of previous ocean drilling legs (DSDP and ODP) mentioned in the text. Red triangles mark the locations of active, emergent volcanoes from the Smithsonian Global Volcanism database. (For interpretation of the references to colour in this figure legend, the reader is referred to the web version of this article.)

foundering plate at the time of subduction initiation. In this context, FAB were interpreted to mark the first step in the geological and geochemical succession that created the protoarc. This succession began with FAB and progressed initially to more depleted, transitional compositions, and eventually to boninites, which are the most depleted of arc volcanic rocks, and which show all of the classic trace element indicators of subduction magmatism (Reagan et al., 2010; Ishizuka et al., 2011). However, FAB do not clearly express many of the common geochemical enrichments that are characteristic of arc basalt, such as elevated Th/La, La/Sm, and Nd/Hf. Indeed, these parameters most often appear more depleted in FAB than in average MORB (Reagan et al., 2010) and as such, they do not carry clear evidence of subduction influence in their trace element patterns.

3. SAMPLES, DATA, AND ANALYTICAL METHODS

We report new geochemical data for samples collected by drilling just west of the KPR at Sites U1438, 1201, and 447, and from FAB collected by submersible by

DeBari et al. (1999) from the inner wall of the modern IBM trench at ~32°N (Fig. 1). Petrographic descriptions of the Site U1438 samples are reported in Hickey-Vargas et al. (2018) and by Arculus et al. (2015a). Descriptions of Site 447 and 1201 basalts may be found in Zakariadze et al. (1981) and Savov et al. (2006).

We also report isotopic data for andesitic sills intruding the sedimentary rock unit that immediately overlies basement at Site U1438. The age of the sedimentary rocks intruded by the sills appears to be 38–49 Ma, based on bracketing from biostratigraphy and the 49 Ma age of the underlying basement (Ishizuka et al., 2018). The sills occur in three closely spaced layers, each several cm thick, at a distance of 49–55 m above the basement contact. The rocks are sparsely phyric with phenocrysts of clinopyroxene only. Their ages are not known but petrographic observations provide evidence of interaction between melt and soft sediment at the contacts, suggesting that the ages of the sills may be close to the depositional age of the sediments. Additional details about the occurrence are reported in Arculus et al. (2015a). Major and trace element data for these samples is reported by Ishizuka et al. (2018) and Hickey-Vargas et al. (2018).

Throughout the paper we refer to basement rocks from Sites U1438, 1201 and 447 (Fig. 1) as the *west-of-KPR drill site samples* or more simply as the *drill site* or *West-of-KPR samples*. We contrast the compositions of these rocks with data from *FAB samples* of DeBari et al. (1999), Reagan et al. (2010) and Ishizuka et al. (2011). The FAB samples were collected by submersible from the inner trench wall at the locations indicated in Fig. 1 and by drilling at DSDP Sites 458 and 459. Six samples identified by Reagan et al. (2010) as transitional between FAB and boninite have been excluded from our plots because they do not fall unambiguously into the FAB geochemical category as defined by Reagan et al. (2010).

As mentioned above, the age of Site U1438 basement was recently determined by $^{40}Ar/^{39}Ar$ to be ~49 Ma (Ishizuka et al., 2018). Radioisotopic ages for Site 447 and 1201 samples are not available, but patterns in seafloor magnetic anomalies and related constraints indicate that basement ages are no older than ~44 Ma at Site 447 and ~46 Ma at Site 1201 (Hilde and Lee, 1984; Salisbury et al., 2006; Richter and Ali, 2015; Westerhold et al., 2015). Radioisotopic ages are not available for the DeBari et al. (1999) FAB, so for the purposes of this paper, we assume they are similar to other IBM trench-wall basalts and were produced in the 48–52 Ma time window (Ishizuka et al., 2011). Additional background information on Sites 447 and 1201 are available in ocean drilling reports and in follow-up studies of basement rocks (Mattey et al., 1981; Shipboard_Scientific_Party, 1981; Zakariadze et al., 1981; Salisbury et al., 2006; Savov et al., 2006). Drilling results from Expedition 351 at Site U1438 are summarized by Hickey-Vargas et al. (2018) and (Ishizuka et al., 2018) and in more detail by Arculus et al. (2015a).

Following completion of Expedition 351, whole-rock major element compositions were determined by X-ray fluorescence (XRF) on 101 rock powders (ground in agate) from Site U1438. These data were collected at the Geological Survey of Japan. A complete description of the XRF sample preparation steps is provided in Ishizuka et al. (2018). Aliquots of these powders were distributed to co-authors for trace element and isotopic measurements. New analytical results reported here for Site 447, 1201, and forearc rocks were obtained on samples used in prior studies (Hickey-Vargas, 1998; DeBari et al., 1999; Hickey-Vargas et al., 2006; Savov et al., 2006). Trace element analytical methods are described in Hickey-Vargas et al. (2018). Analytical methods for isotopic measurements are summarized below.

Isotope ratios for Nd and Hf were measured in the Center for Elemental Mass Spectrometry at the University of South Carolina. Approximately 300 mg of rock powder was weighed into Teflon capsules and leached for 30 min in closed capsules with 6 N HCl at 90–100 °C. Samples were then rinsed in 18 MΩ H_2O, and the remaining solids were digested for 24 h in a 3:1 HF:HNO_3 mixture. The digested samples were then uncapped and heated gently on a hot plate to incipient dryness. Approximately 5 ml of concentrated HNO_3 was then added. The capsules were sealed and heated to ~90 °C for 1 hour, then uncapped and heated again to dryness. This step was repeated 3 times to remove fluoride precipitates. After the final digestion steps, the samples were rinsed into centrifuge tubes with ~5 mL of 6 N HCl and centrifuged for 10 min at 10,000 rpm. Separate aliquots were pipetted for Nd and Hf column chemistry. Neodymium was isolated using standard cation exchange procedures. The bulk sample was processed though TRU-spec resin (Eichrom) in HNO_3 to separate a rare-earth element cut. Neodymium was separated from this cut using LN-spec resin in HCl (e.g., Pin and Zalduegui, 1997). Hafnium was separated using the method of Münker et al. (2001).

Hafnium and Nd isotope ratios were measured using a ThermoFinnigan Neptune MC-ICP-MS in the Center for Elemental Mass Spectrometry at the University of South Carolina. Solutions were introduced with a 100 µl self-aspirating Teflon nebulizer (ESI, USA) coupled to an ESI APEX-Q system using a Jet sample cone and X-skimmer cone. The samples were diluted to achieve a signal of 2–5 V on ^{143}Nd and ^{176}Hf, and 30–45 analyses were run on each sample, depending on sample volume. Samples were bracketed every 4–6 solutions by the La Jolla standard for Nd, and the JMC-457 standard for Hf. Results were normalized to a $^{143}Nd/^{144}Nd$ value of 0.511858 for La Jolla, and a $^{176}Hf/^{177}Hf$ value of 0.282160 for JMC-475. Results are reported in Tables 1 and 2. Repeat analysis of USGS rock standards run as unknowns (BHVO-2, BCR-2, AGV-1) agree with published reference values of Weis et al. (2006, 2007) to within 0.0–0.4 epsilon units (Supplementary Table 1). Epsilon values (ε_{Nd}, ε_{Hf}) were calculated with a CHUR value of 0.512630 for $^{143}Nd/^{144}Nd$ and 0.282785 for $^{176}Hf/^{177}Hf$ (Bouvier et al., 2008). Procedural blanks, prepared with each round of samples had an average voltage of 0.0013 V for ^{143}Nd and 0.0049 V for ^{176}Hf, indicating an insignificant amount of contamination from processing.

Because Pb abundances in Site U1438 basement basalt samples are low (<0.5 ppm, Hickey-Vargas et al., 2018) and susceptible to effects of seawater alteration and/or contamination during rock powder sample preparation, we measured Pb isotopes on ~200 mg of hand-picked rock chips, which were leached in 6 N HCl at ~110 °C for one hour. These were selected to produce coverage throughout the drill core and focusing on the least-altered samples at each depth. The leached samples were rinsed in 18 MΩ H_2O and digested in Teflon capsules for 24 h in a 3:1 HF:HNO_3 mixture. The Pb was extracted using conventional HNO_3-HBr extraction techniques in anion resin (e.g., Abouchami et al., 1999). Lead isotope ratios were also measured on the Thermo Finnigan Neptune ICP-MS in the Center for Elemental Mass Spectrometry at the University of South Carolina using the Tl addition technique (White et al., 2000). Isotope ratios were corrected for fractionation using $^{203}Tl/^{205}Tl = 0.418911$ and the exponential law. Average ratios measured on NBS 981 standard solutions were $^{206}Pb/^{204}Pb = 16.9355 \pm 0.0008$, $^{207}Pb/^{204}Pb = 15.4894 \pm 0.0009$, $^{208}Pb/^{204}Pb = 36.6939 \pm 0.0030$ (2 standard errors, n = 11). Sample compositions were corrected for instrumental bias using reference values for NBS 981 reported by Todt et al. (1996).

To counteract effects of seawater alteration on Sr isotopes, 150–200 mg aliquots of rock powder were subject to repeated leaching steps prior to analysis. The leaching steps, which were in 14 M HNO_3 in Teflon vials at ~100 °C, were carried out in 1, 3 and 6-hour time increments, followed by rinses in 18 MΩ H_2O. Isotope ratios for Sr in the leached samples were analyzed both at the University of Geneva (Switzerland) and University of South Carolina (USA). Strontium isotope methods used in the Center for Elemental Mass Spectrometry at the University of South Carolina are summarized in Yogodzinski et al. (2015). Methods used in the Department of Earth Sciences at University of Geneva are described in detail in Chiaradia et al. (2011) and Beguelin et al. (2015). These methods are briefly summarized below.

The leached samples were dissolved for 7 days in Teflon vials using 4 ml of concentrated HF and 1 ml of 14 M HNO_3 at 140 °C. The samples were sonicated twice daily for 30 min during the 7-day digestion. The digested samples were then dried and re-dissolved for 3 days in 3 ml of 14 M HNO_3 and dried again. Strontium was separated from the leached and digested samples using cascade columns with Sr-Spec resins according to a protocol modified from that of Pin et al. (1994). The purified Sr was redissolved in 2% HNO_3 solutions and $^{87}Sr/^{86}Sr$ ratios were measured using a Thermo Neptune PLUS Multi-Collector ICP-MS in static mode. The $^{88}Sr/^{86}Sr = 8.375209$ ratio was used to correct for internal fractionation. SRM987 was used as an external standard to correct measurements on unknowns to a common value of $^{87}Sr/^{86}Sr = 0.710248$ (long-term external reproducibility: 10 ppm). Interferences at masses 84 (^{84}Kr), 86 (^{86}Kr) and 87 (^{87}Rb) were corrected by monitoring ^{83}Kr and ^{85}Rb. Total procedural blanks were <100 pg for Sr.

4. RESULTS

Hafnium and Nd isotopes are reported in Table 1 for IODP Site U1438 samples and in Table 2 for basement samples from DSDP Site 447 and ODP Site 1201. New Hf and Nd isotope data for FAB collected from the northern IBM inner trench wall at ~32°N (samples of DeBari et al., 1999) are also reported in Table 2. Age-corrected compositions at 49 Ma are less radiogenic than measured (present-day) values by 0.1–0.5 epsilon units (Tables 1 and 2). These offsets are, at most, only slightly greater than analytical precision of ~0.3 epsilon units based on sample replicates and repeat analyses of rock standards (Supplementary Table 1). For this reason, and to simplify comparisons to middle and late Cenozoic datasets, Hf and Nd isotopes plotted in Figs. 2 and 3 and throughout this paper are the measured values.

Site U1438 basement basalts have Hf and Nd isotopes that are relatively radiogenic and well correlated, from ε_{Hf} of +14.5 to +19.5 and ε_{Nd} of +7.5 to +9.8 (Fig. 2a). Compositions become somewhat less radiogenic and more variable with time, from the bottom of the basement section to the top (Fig. 3a–b). The andesite sills that intrude sedimentary rocks overlying basement at Site U1438 fall at the less radiogenic end of basement basalt data range with ε_{Hf} of +13.6 to +14.0 and ε_{Nd} from +6.0 to +7.5 (Fig. 2a). All of the basement basalts of Unit 1 at Site U1438 have compositions that fall within the Indian-MORB field in Hf-Nd isotope space. Site 1201 basement basalts and northern IBM FAB are indistinguishable from Site U1438 basement with respect to Hf and Nd isotopes (Fig. 2a). Basement at Site 447 is more variable and includes some samples with more radiogenic Nd relative to Hf, but the combined dataset for drill site basement samples immediately west of the KPR (Sites U1438, 1201 and 447) all cluster within ±2 epsilon units of $\varepsilon_{Hf} = 18$ and $\varepsilon_{Nd} = 9.5$ (Fig. 2). The FAB samples of Reagan et al. (2010) and Ishizuka et al. (2011a) are slightly more variable with respect to ε_{Nd} and are never as radiogenic in terms of ε_{Hf} (data from Reagan et al., 2010 only) but do not occupy isotopic space significantly different than that defined by basement samples west of the KPR at sites U1438, 1201 and 447 (Fig. 2b).

Lead isotopes for IODP Site U1438 samples are reported in Table 3. Age-corrections to 49 Ma reduce $^{206}Pb/^{204}Pb$ by an average of 0.2 units compared to present-day values and have a negligible affect on $^{207}Pb/^{204}Pb$ and $^{208}Pb/^{204}Pb$ (Table 3). Because U abundances in Site U1438 and FAB samples are likely to have been affected to varying degrees by seawater alteration (Shipboard_Scientific_Party, 1981; Savov et al., 2006; Hickey-Vargas et al., 2018) Pb isotopes plotted in Fig. 4 are measured values only.

Lead isotopes for Site U1438 samples are well correlated in plots of $^{207}Pb/^{204}Pb$ (not shown) and $^{208}Pb/^{204}Pb$ versus $^{206}Pb/^{204}Pb$ (Fig. 4). As in the case of Hf and Nd, the Pb isotopes become somewhat less depleted (i.e., increase in $^{208}Pb/^{204}Pb$) upward through the basement section (Fig. 3c). Consistent with Hf and Nd isotope results, basement basalts from sites U1438, 1201 and 447 all have elevated $^{208}Pb/^{204}Pb$ and mostly fall within the Indian-

Table 1
Hf-Nd Isotopes for Site U1438 Samples.

	Depth (mbsf)	Basement subunit*	$^{143}Nd/^{144}Nd$	± 2SE†	ε_{Nd}††	$^{176}Hf/^{177}Hf$	± 2SE†	ε_{Hf}††	Sm	Nd	Lu	Hf	Sm/Nd	Lu/Hf	$^{143}Nd/^{144}Nd$ t = 49 Ma†††	ε_{Nd} t = 49 Ma†††	$^{176}Hf/^{177}Hf$ t = 49 Ma†††	ε_{Hf} t = 49 Ma†††
Site U1438 Andesite Sills																		
1438E61R2 3–5	1406.38		0.513013	5	7.5	0.283170	6	13.6	2.26	9.84	0.226	1.01	0.230	0.223				
1438E61R2 92–95	1407.28		0.512942	5	6.1	0.283174	4	13.7	2.97	11.8	0.293	1.35	0.252	0.216				
1438E61R2 95–97	1408.28		0.512979	4	6.8	0.283175	4	13.8										
1438E62R1 124–126	1411.55		0.512962	4	6.5	0.283182	3	14.0	2.62	9.85	0.232	0.921	0.266	0.252				
Site U1438 Basement Basalts																		
1438E69R1 98–101	1461.90	1a	0.513093	6	9.0	0.283296	5	18.1	1.71	4.57	0.288	1.09	0.375	0.264	0.513021	8.8	0.283262	18.0
1438E70R2 16–19	1466.70	1a	0.513076	4	8.7	0.283293	3	18.0	1.98	5.28	0.304	1.42	0.375	0.214	0.513004	8.5	0.283265	18.1
1438E71R1 98–101	1471.10	1a	0.513087	5	8.9	0.283293	2	17.9	1.78	4.67	0.294	1.17	0.382	0.252	0.513013	8.7	0.283260	17.9
1438E71R3 101–104	1473.76	1b	0.513085	11	8.9	0.283257	4	16.7	1.74	4.18	0.312	1.13	0.416	0.276	0.513004	8.5	0.283221	16.5
1438E71R3 101–104 (rep)	1473.76	1b	0.513080	6	8.8	0.283254	4	16.6	1.74	4.18	0.312	1.13						
1438E72R1 145–148	1476.17	1b	0.513087	22	8.9	0.283254	5	16.6	2.01	4.69	0.314	1.18	0.428	0.266	0.513004	8.5	0.283220	16.5
1438E73R2 123–128	1486.85	1b	0.513036	6	7.9	0.283231	4	15.8	1.51	3.79	0.361	0.991	0.399	0.364	0.512959	7.6	0.283184	15.2
1438E74R2 21–24	1495.71	1c	0.513056	5	8.3	0.283272	3	17.2	2.22	5.54	0.415	1.40	0.400	0.297	0.512978	8.0	0.283233	16.9
1438E75R1 81–85	1504.63	1c	0.513080	4	8.8	0.283296	4	18.1	2.07	5.29	0.406	1.40	0.392	0.290	0.513004	8.5	0.283258	17.8
1438E75R1 81–85 (rep)	1504.63	1c	0.513083	6	8.8	0.283297	4	18.1	2.07	5.29	0.406	1.40	0.392	0.290	0.513007	8.6	0.283259	17.9
1438E76R2 86–91	1509.10	1c	0.513073	4	8.6	0.283285	6	17.7	1.97	4.95	0.384	1.35	0.398	0.284	0.512996	8.4	0.283248	17.5
1438E76R3 105–110	1510.75	1c	0.513074	4	8.7	0.283296	6	18.1	1.85	4.59	0.352	1.22	0.403	0.289	0.512995	8.4	0.283259	17.8
1438E77R1 53–58	1511.36	1c	0.513070	6	8.6	0.283293	4	18.0	1.97	5.00	0.379	1.34	0.393	0.284	0.512994	8.3	0.283256	17.8
1438E77R3 41–43	1513.60	1c	0.513062	7	8.4	0.283278	3	17.4	2.04	4.96	0.385	1.31	0.411	0.294	0.512982	8.1	0.283240	17.2
1438E77R3 41–43 (rep)	1513.60	1c	0.513064	5	8.5	0.283272	3	17.2	2.04	4.96	0.385	1.31						
1438E78R2 127–130	1518.09	1c	0.513059	9	8.4	0.283275	4	17.3	1.68	4.16	0.326	1.07	0.404	0.304	0.512980	8.1	0.283236	17.0
1438E78R4 49–53	1520.12	1c	0.513017	14	7.5	0.283195	8	14.5	1.91	4.73	0.381	1.29	0.403	0.295	0.512939	7.2	0.283156	14.2
1438E78R4 52–53	1520.13	1c	0.513018	8	7.6	0.283200	3	14.7										
1438E78R4 52–53 (rep)	1520.13	1c	0.513002	6	7.3	0.283200	4	14.7										
1438E79R2 6–11	1525.55	1c	0.513019	10	7.6	0.283191	4	14.4	1.84	4.60	0.377	1.25	0.401	0.301	0.512941	7.3	0.283152	14.1
1438E79R4 48–53	1528.75	1c	0.513073	7	8.6	0.283292	5	17.9	2.22	5.69	0.423	1.46	0.391	0.290	0.512997	8.4	0.283255	17.7
1438E80R2 27–30	1535.27	1d	0.513088	11	8.9	0.283279	6	17.5	1.88	4.56	0.353	0.956	0.413	0.369	0.513008	8.6	0.283231	16.9
1438E81R1 114–119	1544.07	1d	0.513084	5	8.9	0.283269	6	17.1	1.87	4.63	0.365	1.24	0.403	0.294	0.513006	8.6	0.283231	16.8
1438E82R1 61–66	1552.64	1d	0.513077	5	8.7	0.283284	5	17.6	1.91	4.59	0.363	1.23	0.416	0.296	0.512996	8.4	0.283245	17.4
1438E82R3 77–80	1555.49	1d	0.513099	11	9.2	0.283275	4	17.3	1.83	4.63	0.357	1.25	0.396	0.286	0.513023	8.9	0.283238	17.1
1438E83R1 112–115	1562.54	1d	0.513119	4	9.5	0.283277	3	17.4	1.85	4.47	0.352	1.20	0.414	0.293	0.513039	9.2	0.283239	17.1
1438E83R1 112–115 (rep)	1562.54	1d	0.513122	16	9.6	0.283280	8	17.5	1.85	4.47	0.352	1.20	0.414	0.293	0.513041	9.3	0.283242	17.3
1438E83R1 132–136	1562.74	1d	0.513106	5	9.3	0.283276	6	17.4	1.88	4.58	0.351	1.26	0.411	0.280	0.513027	9.0	0.283240	17.2
1438E83R3 8–10	1564.31	1d	0.513102	13	9.2	0.283282	4	17.6	1.93	4.61	0.365	1.29	0.419	0.284	0.513020	8.8	0.283245	17.3
1438E84R1 96–99	1572.08	1e	0.513124	6	9.6	0.283336	3	19.5	1.40	3.22	0.293	0.867	0.435	0.338	0.513040	9.2	0.283292	19.0
1438E85R1 45–47	1579.56	1e	0.513121	5	9.6	0.283336	3	19.5	1.35	3.17	0.274	0.867	0.425	0.316	0.513039	9.2	0.283295	19.1
1438E85R1 124–127	1580.36	1e	0.513132	6	9.8	0.283344	6	19.8	1.36	3.15	0.288	0.877	0.431	0.328	0.513048	9.4	0.283301	19.3
1438E86R1 25–28	1585.17	1e	0.513126	4	9.7	0.283331	6	19.3	1.40	3.29	0.296	0.864	0.425	0.343	0.513043	9.3	0.283287	18.8
1438E86R2 13–16	1586.41	1e	0.513116	18	9.5	0.283333	4	19.4	1.38	3.31	0.292	0.864	0.418	0.338	0.513035	9.1	0.283289	18.9
1438E87R1 12–15	1594.14	1e	0.513121	3	9.6	0.283322	4	19.0	1.35	3.10	0.283	0.884	0.435	0.320	0.513036	9.2	0.283280	18.6
1438E87R1 115–118	1595.17	1e	0.513118	4	9.5	0.283332	3	19.3	1.53	3.50	0.330	0.980	0.436	0.337	0.513034	9.1	0.283288	18.9
1438E87R3 56–60	1596.40	1e	0.513130	6	9.8	0.283341	6	19.7	1.38	3.16	0.286	0.868	0.436	0.329	0.513046	9.3	0.283298	19.2
1438E88R1 142–145	1604.54	1f	0.513128	7	9.7	0.283297	4	18.1	1.76	4.06	0.349	1.18	0.434	0.296	0.513044	9.3	0.283259	17.8

* Basement subunit intervals are fromHickey-Vargas et al. (2018).

† Uncertainties (±) for isotope ratios reflect within-run variation calculated as 2σ standard errors (SE) and expressed as variation in the 6th decimal place.

†† Epislon values calculated with chondritic ratios of $^{176}Hf/^{177}Hf = 0.282758$ and $^{143}Nd/^{144}Nd = 0.512630$ (Bouvier et al., 2008).

††† Age corrections to 49 Ma use chondritic values for (CHUR) from Bouvier et al. (2008). No corrections are shown for andesite sill samples because their age is not known.

MORB field where they fill effectively the same compositional space as FAB with $^{206}Pb/^{204}Pb$ from 17.8 to 18.8 (Fig. 4). The andesite sill samples from Site U1438 lie at the radiogenic end of this data range. The least radiogenic Pb isotopes in the FAB and west-of-KPR drill site samples are like those of Shikoku and Parece-Vela backarc basalts, with $^{206}Pb/^{204}Pb$ less than 18.1. Radiogenic Pb isotope compositions ($^{206}Pb/^{204}Pb > 18.8$), which are common in volcanic rocks of the modern IBM arc and in plume-influenced basalts (OIB) of the West Philippine Basin (Hickey-Vargas, 1998; 2006) are absent from the Site U1438 and FAB datasets (Fig. 4).

Strontium isotopes in Site U1438 basement rocks are widely variable overall with $^{87}Sr/^{86}Sr$ ratios ranging from 0.7033 to 0.7058 (Table 4). However, most samples have relatively uniform and unradiogenic compositions with $^{87}Sr/^{86}Sr$ ratios between 0.7033 and 0.7038 (Table 4). For the relatively unradiogenic samples, $^{87}Sr/^{86}Sr$ remains constant with depth (age) or becomes only slightly enriched in ^{87}Sr toward the bottom of the Site U1438 section (Fig. 3d), unlike the Hf-Nd-Pb characteristics. In Sr-Nd isotope space (Fig. 5) basement samples from Site U1438 define a horizontal array, but the least radiogenic samples have $^{87}Sr/^{86}Sr < 0.7038$ and are clustered with other drill site and FAB samples at the depleted end of the Indian MORB field (Fig. 4a).

Hickey-Vargas et al. (2018) present new trace element data showing that the highly depleted character of FAB is also present in Site U1438 basement rocks which are most depleted in the lower basement subunits and less depleted in the middle and upper subunits. Basement subunit boundaries are shown in Fig. 3 and listed in Table 1. This change in time is particularly clear in subunit 1e samples, which have lower incompatible element abundances and more depleted patterns than samples from the overlying subunits 1b-1d (Fig. 6a). Samples in subunit 1a at the top of the basement section have been affected by hydrothermal alteration and by interaction with overlying metalliferous sediment (Hickey-Vargas et al., 2018) and are not shown in Fig. 6. Samples from all other basement sub-units at Site U1438 are clearly more depleted than Pacific MORB. A similar change in time at Site U1438 is also seen in Hf and Nd isotopes, which are more variable and less radiogenic on average in the middle and upper subunits compared to the bottom (Fig. 3a–b). Some alteration-resistant trace element ratios (La/Yb, Lu/Hf, Zr/Nb, Sm/Nd) are also more depleted at the bottom than in the middle and upper subunits (Fig. 7 in Hickey-Vargas et al., 2018). At Site U1438, only the andesite sills show the characteristic depletions and enrichments of common, subduction-related volcanic rocks (Fig. 11 in Hickey-Vargas et al., 2018).

The depleted character of the west-of-KPR drill site samples, equivalent to those of FAB, is well expressed in basement rocks from Site 1201 (see also Savov et al., 2006), which have lower incompatible element abundances and more depleted patterns than nearly all Pacific MORB (Fig. 6b). Basement samples from Site 447 are somewhat less depleted, but nonetheless lie at the depleted end of the Pacific MORB field (Fig. 6c).

A more complete comparison for all available data is illustrated in Fig. 7, which shows that FAB and basement samples from Sites U1438, 1201 and 447 are similar and express more depleted trace element compositions than are generally seen even in large MORB data sets. We focus on La, Hf and Ti abundances because these elements are resistant to alteration and because they express a wide range of incompatible behavior in magmatic systems. It is evident from Fig. 7 that the FAB and west-of-KPR basement rocks are more depleted in these elements than most Indian and Pacific MORB (Fig. 7a–c). The ratios La/Yb and Hf/Lu are chosen because they express the shapes of the incompatible element patterns shown in Fig. 6, but in a format where larger numbers of samples may be shown. These ratios show to an even greater extent than trace element abundances, the highly depleted character of the FAB and west-of-KPR drill sites basement samples compared to Pacific and Indian MORB (Fig. 7e–h).

5. DISCUSSION

5.1. A common source for Eastern, West Philippine basement and FAB

Comparison of basement basalts from the drill sites immediately west of the KPR (Sites U1438, 1201 and 447) with FAB indicate that all were derived from a similar highly depleted mantle source. Collectively, the drill site basement rocks and FAB data sets are indistinguishable with respect to Hf isotopes (ε_{Hf} mostly >16.0), which are more radiogenic than most Pacific and Indian MORB (Fig. 2). Lead isotopes for the FAB and drill site data sets (Fig. 4) are also effectively the same and unlike most IBM arc rocks or plume-related basalts of the West Philippine Basin such as those discussed by Hickey-Vargas (1991, 1998) and Ishizuka et al. (2013). Interpretation of $^{87}Sr/^{86}Sr$ is less straightforward because wide scatter in Site U1438 data to values >0.704 in samples with uniformly radiogenic Nd (ε_{Nd} ~9.0 – Fig. 5) indicate that there has been a significant role for seawater alteration in some samples (see Hickey-Vargas et al., 2018, for full discussion of alteration in Site U1438 basement). Despite these effects, the clear inverse correlation in Nd-Sr isotope space for most FAB and drill sites samples along the high-ε_{Nd} edge of the Indian-MORB field in Fig. 5a is likely an expression of mantle source. This includes west-of-KPR drill site and FAB samples with ε_{Nd} from 8.0 to 11.0 and excludes samples with $^{87}Sr/^{86}Sr$ >0.7034, which may have been affected by alteration. We conclude that drill site basement rocks occupy the same isotopic space as FAB for Hf, Nd, Sr and Pb.

The distinctive nature of the west-of-KPR drill site basement and FAB samples is also well expressed in trace element data plotted in Fig. 7. Comparisons are made to Indian and Pacific (Gale et al., 2013) and to normal MORB values (Arevalo and McDonough, 2010). For example, median La/Yb in basement samples from Site U1438 (0.48), Site 1201 (0.60) and in FAB (0.54) are more depleted than 95% of data for Pacific and Indian MORB compiled by Gale et al. (2013) which have median La/Yb = 1.14

Table 2
Hf-Nd Isotopes for Site 1201, Site 447 and 32° N FAB.

Sample	$^{143}Nd/^{144}Nd$	± 2SE[†]	ε_{Nd}[††]	$^{176}Hf/^{177}Hf$	± 2SE[†]	ε_{Hf}[††]	Sm	Nd	Lu	Hf	Sm/Nd	Lu/Hf	$^{143}Nd/^{144}Nd$ (t)[†††]	ε_{Nd} (t)[†††]	$^{176}Hf/^{177}Hf$ (t)[†††]	ε_{Hf} (t)[†††]
ODP Site 1201 Basement Basalts[*]																
1201D-46R-3 (43–45)	0.513054	7	8.3	0.283252	4	16.5	2.03	6.00	0.44		0.34		0.512991	8.2		
1201D-46R-5 (6–8)	0.513077	7	8.7	0.283256	3	16.6	2.21	6.31	0.40	2.26	0.35	0.177	0.513012	8.6	0.283234	17.7
1201-48R-2 (92–94)	0.513134	4	9.8	0.283321	4	19.0	2.08	5.25	0.37	1.35	0.40	0.274	0.513060	9.6	0.283287	20.0
1201D-48R-4 (66–68)	0.513143	4	10.0	0.283315	5	18.7	2.12	5.33	0.39	1.39	0.40	0.277	0.513069	9.7	0.283280	19.8
1201D-49R-1 (11–13)	0.513148	5	10.1	0.283325	5	19.1	1.98	5.04	0.36	1.33	0.39	0.269	0.513075	9.9	0.283291	20.1
1201D-49R-1 (47–49)	0.513139	3	9.9	0.283329	5	19.2	2.06	5.16	0.37	1.37	0.40	0.271	0.513065	9.7	0.283296	20.3
1201D-49R-3 (37–39)	0.513135	6	9.9	0.283316	4	18.8	2.09	5.29	0.39	1.40	0.40	0.278	0.513061	9.6	0.283281	19.8
1201D-51R-1 (2–4)	0.513136	4	9.9	0.283315	4	18.7	2.03	5.10	0.37	1.35	0.40	0.274	0.513062	9.6	0.283281	19.8
1201D-52R-2 (56–58)	0.513142	6	10.0	0.283328	4	19.2	1.88	4.71	0.34	1.28	0.40	0.267	0.513068	9.7	0.283295	20.2
1201D-53R-1 (119–121)	0.513139	4	9.9	0.283324	4	19.1	2.05	5.17	0.38	1.37	0.40	0.275	0.513065	9.7	0.283290	20.1
1201D-65R-1 (47–49)	0.513141	4	10.0	0.283330	4	19.3	2.02	5.09	0.36	1.34	0.40	0.269	0.513067	9.7	0.283297	20.3
DSDP Site 447 Basement Basalts[**]																
447A 14-1	0.513128	5	9.7	0.283249	4	16.4										
447A-14-2 (2–4)	0.513140	5	9.9	0.283248	4	16.4	2.39	6.74	0.40	1.67	0.35	0.238	0.513078	9.8	0.283220	17.3
447A-16-2 (22–24)	0.513174	7	10.6	0.283290	4	17.9	2.24	6.56	0.37	1.56	0.34	0.236	0.513115	10.6	0.283262	18.8
447A -17-2 (1–4)	0.513137	5	9.9	0.283297	4	18.1	3.00	8.12	0.53	2.01	0.37	0.265	0.513073	9.7	0.283266	19.1
447A-17-2 (53–55)	0.513128	6	9.7	0.283293	5	18.0	2.94	7.84	0.54	2.08	0.37	0.259	0.513063	9.6	0.283263	18.9
447A-17-3 (105–107)	0.513154	6	10.2	0.283293	4	18.0	2.84	7.64	0.52	1.98	0.37	0.263	0.513089	10.1	0.283262	18.9
447A-21-1 (128–130)	0.513150		10.1	0.283306	3	18.4	2.25	5.78	0.43	1.59	0.39	0.267	0.513082	9.9	0.283275	19.4
447A-22-1 (60–62)	0.513152	6	10.2	0.283314	3	18.7	2.21	5.69	0.42	1.52	0.39	0.276	0.513084	10.0	0.283282	19.7
447A 22R-3 (18–20)	0.513185		10.8	0.283290		17.9										
447A-23-1 (16–19)	0.513178	6	10.7	0.283296	4	18.1	2.40	6.21	0.43	1.66	0.39	0.257	0.513111	10.5	0.283266	19.0
447A 24-2	0.513175	6	10.6	0.283264	3	16.9										
447A 25-1 (15–17)	0.513162	6	10.4	0.283265	4	17.0										
447A-25-1 (9–11)	0.513155		10.2	0.283275		17.3	1.83	5.13	0.30	1.28	0.36	0.237	0.513093	10.1	0.283247	18.3
447A-30-2 (80–82)	0.513096		9.1	0.283268	4	17.1	1.92	5.32	0.34	1.37	0.36	0.250	0.513033	9.0	0.283238	18.0
Submersible Samples - Trench Wall Forearc Basalts (FAB)[***]																
150-01	0.513080	2	8.8	0.283259	2	16.8	3.69	8.96	0.61	2.54	0.41	0.240	0.512999	8.4	0.283227	17.9
150-02	0.513081	2	8.8	0.283255	3	16.6	3.58	8.40	0.61	2.34	0.43	0.261	0.512997	8.4	0.283221	17.7
150-03	0.513086	2	8.9	0.283261	3	16.8	3.61	8.40	0.65	2.27	0.43	0.286	0.513001	8.5	0.283223	17.9
BT-1	0.513094	2	9.0	0.283284	4	17.6	1.41	3.05	0.27	0.81	0.46	0.333	0.513002	8.5	0.283240	18.8
BT-2	0.513086	2	8.9	0.283250	3	16.5	2.66	6.16	0.48	1.68	0.43	0.286	0.513001	8.5	0.283212	17.6
169-01a	0.513084	2	8.9	0.283279	1	17.5	1.84	4.31	0.35	1.16	0.43	0.302	0.513000	8.5	0.283239	18.6
169-01b	0.513091	2	9.0	0.283279	2	17.5	1.83	4.20	0.35	1.07	0.44	0.327	0.513005	8.6	0.283236	18.6

[*] Site 1201 samples are from Savov et al. (2006) with Hf isotopes from this study. Nd isotopes are from Savov et al. (2006) except samples 46R-3 and 46R-5 from this study. Trace elements are from Table 5 except for 46R-3 and 46R-5 from Savov et al. (2006).

[**] Site 447 data are from this study except Nd isotopes for samples 21-1 and 30-2 which are from Hickey-Vargas (1991). Data for sample 25-1 are from Hickey-Vargas (2006) with correction based on JMC standard $^{176}Hf/^{177}Hf = 0.282160$. Data for sample 22R-3 are from Pearce et al. (1999).

[***] Submersible samples from trench wall (FAB) are from DeBari et al. (1999). Hf and Nd isotopes are from this study. Trace elements are from DeBari et al. (1999).

[†] Uncertainties (±) reflect within-run variation calculated as 2σ standard errors (SE) and expressed as variation in the 6th decimal place.

[††] Epsilon values calculated with chondritic ratios of $^{176}Hf/^{177}Hf = 0.282758$ and $^{143}Nd/^{144}Nd = 0.512630$ (Bouvier et al., 2008).

[†††] Corrections to initial compositions assume ages of ~47 Ma for Site 1201, ~44 Ma for Site 447, and ~50 Ma for FAB, using chondritic values for (CHUR) fromBouvier et al. (2008).

Table 3
Pb Isotopes for Site 1438 Samples [*]

	Depth (mbsf)	Rock Type	$^{206}Pb/^{204}Pb$	± 2SE[†]	$^{207}Pb/^{204}Pb$	± 2SE[†]	$^{208}Pb/^{204}Pb$	± 2SE[†]	Pb	Th	U	U/Pb	Th/Pb	$^{206}Pb/^{204}Pb$ t = 49 Ma	$^{207}Pb/^{204}Pb$ t = 49 Ma	$^{208}Pb/^{204}Pb$ t = 49 Ma
Site U1438 Andesite Sills																
1438E61R2 (4–7)	1406.4	andesite	18.6270	4	15.5607	4	38.3969	12	6.62	0.169	0.472	0.071	0.026			
1438E61R2 (97–100)	1408.3	andesite	18.6114	4	15.5547	4	38.3752	12	4.32	0.211	0.326	0.076	0.049			
1438E62R1 (124–126)	1411.6	andesite	18.6333	5	15.5428	5	38.3163	15	2.81	0.153	0.196	0.070	0.055			
Site U1438 Basalt Basement																
1438E69R1 50–51	1461.4	basalt	18.5126	3	15.5015	4			2.397	0.067	0.211	0.088	0.028	18.4924	15.5006	
1438E73R2 (77–74)	1486.3	basalt	18.5184	3	15.5011	4	38.1695	10	0.679	0.031	0.122	0.180	0.046	18.4317	15.4971	38.1622
1438E74R2 21–24	1495.7	basalt	18.3789	7	15.4878	6	38.1866	18	0.614	0.048	0.018	0.029	0.078	18.3648	15.4871	38.1742
1438E76R2 16–18	1439.1	basalt	18.2826	14	15.4791	13	38.1124	38	0.039	0.043	0.017	0.436	1.103	18.0731	15.4693	37.9383
1438E76R2 84–86	1509.1	basalt	18.2651	5	15.4807	5	38.1079	16	0.384	0.048	0.017	0.044	0.125	18.2439	15.4797	38.0881
1438E77R1 88–90	1511.7	basalt	18.2807	8	15.4767	9	38.1000	24	0.125	0.047	0.018	0.144	0.376	18.2116	15.4735	38.0406
1438E82R1 57–59	1552.6	basalt	18.4881	5	15.4960	5	38.1260	12	0.225	0.040	0.078	0.347	0.178	18.3210	15.4882	38.0979
1438E82R2 102–105	1554.4	basalt	18.4811	5	15.4936	7	38.1306	20	0.091	0.036	0.101	1.110	0.396	17.9460	15.4684	38.0679
1438E83R1 111–112	1562.5	basalt	18.4678	8	15.4918	9	38.1303	24	0.470	0.039	0.070	0.149	0.083	18.3960	15.4884	38.1172
1438E83R2 36–38	1563.2	basalt	18.5987	20	15.5062	23	38.0973	64	0.214	0.042	0.221	1.033	0.196	18.1003	15.4828	38.0661
1438E85R1 43–45	1579.6	basalt	18.4059	23	15.4979	20	38.1287	56	0.085	0.018	0.070	0.824	0.212	18.0093	15.4792	38.0952
1438E87R1 116–119	1595.2	basalt	18.2028	4	15.4721	3	38.0460	9	0.304	0.022	0.033	0.109	0.072	18.1508	15.4696	38.0346
1438E88R1 97–98	1604.1	basalt	18.3685	10	15.4891	11	38.0275	37	0.072	0.028	0.095	1.319	0.389	17.7344	15.4593	37.9661

[*] Pb isotopes were determined on leached rock chips. Pb, Th, and U abundances were determined on unleached rock powders. Age corrections should be considered to be approximate values.
[†] Uncertainties (±) reflect within-run variation calculated as 2σ standard errors (SE) and expressed as variation in the 6th decimal place.

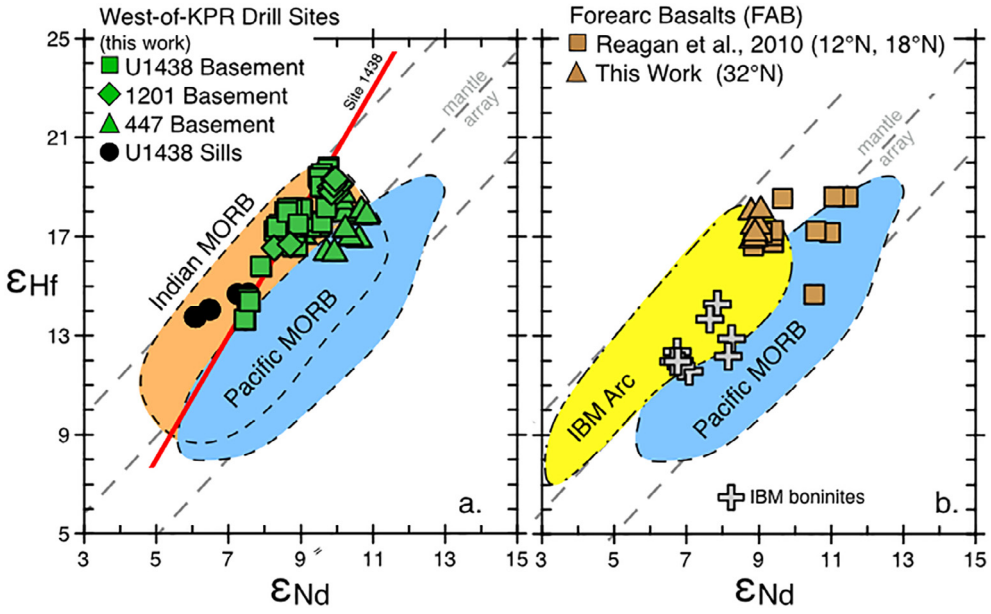

Fig. 2. Plots of ε_{Hf} versus ε_{Nd} comparing Site U1438 samples with Site 1201 and 447 basement basalts and with FAB, MORB and IBM data sets. Site U1438 data are from Table 1. Data for Site 1201 and 447 basement rocks are from Table 2 and include some data from Hickey-Vargas (2005), DeBari et al. (1999), and Savov et al. (2006). New Hf and Nd isotopes presented here for 32°N FAB samples of DeBari et al. (1999) are from Table 2. Pacific and Indian MORB data are from Gale et al. (2013) and other published sources. Data for IBM arc and rearc are from these sources (White and Patchett, 1984; Woodhead, 1989; Pearce et al., 1999; Woodhead et al., 2001; Wade et al., 2005; Kohut et al., 2006; Stern et al., 2006; Tamura et al., 2009; Tollstrup et al., 2010; Tamura et al., 2011; Woodhead et al., 2012). The solid red line is a major-axis regression through Site U1438 basement samples only. Gray dashed lines mark the Hf-Nd isotope mantle array (center line ±4 ε_{Hf} units) of Vervoort and Blichert-Toft (1999). Data for IBM boninites are from Pearce et al. (1999) and Reagan et al. (2010).

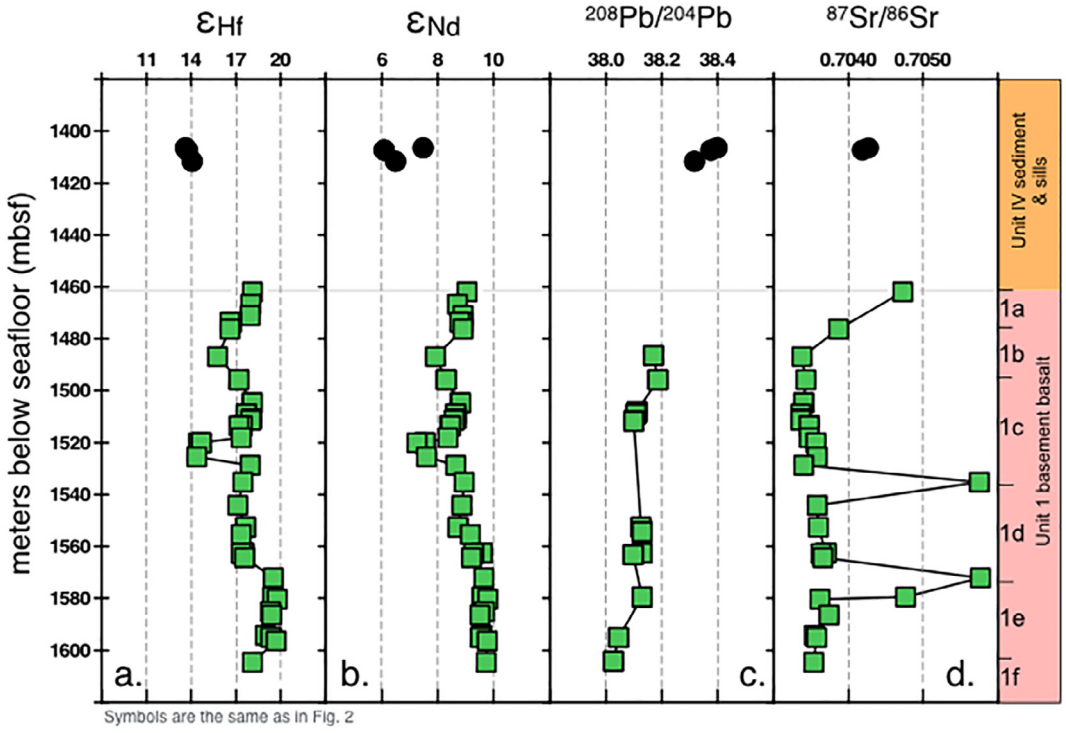

Fig. 3. Whole-rock isotopic compositions (Hf, Nd, Pb, Sr) versus depth for Site U1438 drill core samples. The figure includes Unit 1 basement samples and andesite sills that intrude sedimentary rocks of Unit IV, which overlies basement. Drilling results and unit definitions are summarized by Hickey-Vargas et al. (2018). A full report on Expedition 351 drilling is provided by Arculus et al. (2015a). Hafnium and Nd isotope data are from Table 1. Lead isotopes are from Table 3. Strontium isotope data are from Table 4.

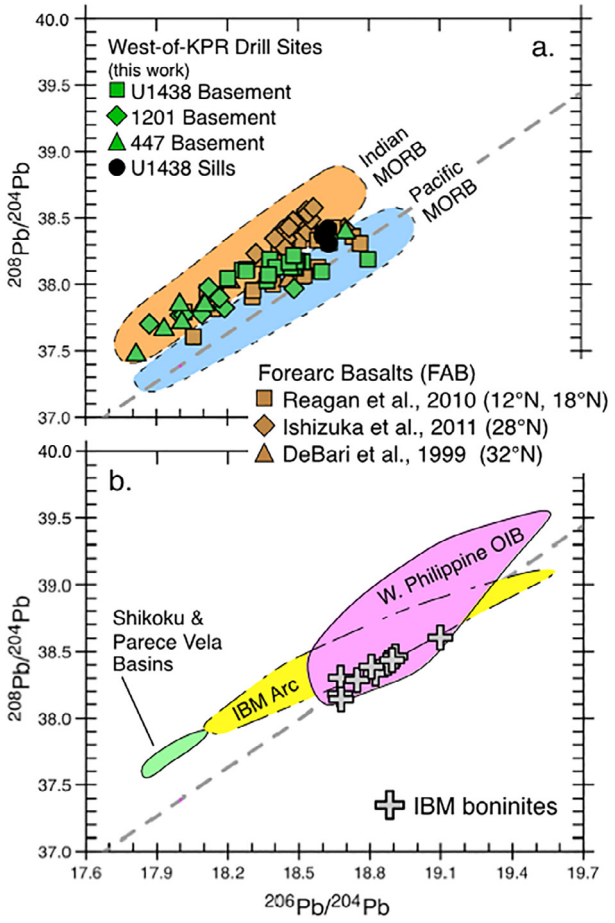

Fig. 4. Plots of $^{208}Pb/^{204}Pb$ versus $^{206}Pb/^{204}Pb$ comparing Site U1438 samples with Site 1201 and 447 basement basalts and with FAB, MORB, IBM arc, and West Philippine data sets. Site U1438 are from Table 3. Forearc basalt (FAB) data are from sources indicated on the figure. Triangular symbols showing the compositions of FAB samples from 32° (DeBari et al., 1999) are obscured by drill site data (green symbols) with $^{206}Pb/^{204}Pb$ from 18.2 to 18.5. West Philippine and Shikoku-Parece Vela data are from Hickey-Vargas et al. (1991, 1998). Sources of other data are indicated in the caption to Fig. 2. Data for IBM boninites are from Pearce et al. (1999) and Reagan et al. (2010). (For interpretation of the references to colour in this figure legend, the reader is referred to the web version of this article.)

(Fig. 7e–f). Site 447 basement basalts are slightly less depleted with median La/Yb = 0.72, but are still in the 90th percentile of Indian and Pacific MORB. With respect to Lu/Hf, FAB is more depleted than 95% of Pacific and Indian MORB, whereas basalts from Site U1438, 1201 and 447 are in the 90th, 85th and 80th percentile respectively (Fig. 7g–h). Thus, the FAB and west-of-KPR drill site data sets are similar and distinctive in that both carry key trace element ratios that are more depleted than 80–95% of MORB in the broader region.

Similar ages around 50 Ma for Site U1438 and 1201 basement rocks (Hilde and Lee, 1984; Richter and Ali, 2015; Ishizuka et al., 2018) and for FAB (Reagan et al., 2010; Ishizuka et al., 2011; Reagan et al., 2017) combined with similar and distinctive trace element and isotopic characteristics (e.g., Figs. 2, 4–7) also indicate that basalts from these locations were produced by melting of the same upper mantle source. This source was sampled widely by volcanism in a broad swath of seafloor across the strike of the protoarc at the site of IBM subduction initiation, and more than 1000 km along-strike, around the time of IBM subduction initiation. Pending improved age constraints for Site 447 basement, which appear to be no more than ~44 million years old based on seafloor magnetic anomalies (Hilde and Lee, 1984; Westerhold et al., 2015), it may also be true that depleted tholeiites with FAB compositions were produced by seafloor spreading in the eastern West Philippine basin several million years after initiation of IBM subduction.

5.2. Depletion History of the Site U1438 and FAB Source

Compositional changes in time through the Site U1438 basement section for trace element and isotope ratios, which are often most depleted at the bottom of the basement section (Fig. 3 here and Fig. 7 in Hickey-Vargas et al., 2018) indicate that trace element depletions in the basement are linked to depletions in their source inferred from the long-lived radiogenic isotopes. The range of compositions in the Site U1438 basement is modest, and there is an anomalous excursion to unradiogenic ε_{Hf} and ε_{Nd} at 1525 mbsf (Fig. 3a–b), but the linked nature of changes with time in a variety of trace element ratios and in Nd, Hf and Pb isotopes through the section is unmistakable (Fig. 3 here and Fig. 7 in Hickey-Vargas et al., 2018).

The coherence of the pattern with time implies that most Site U1438 samples were produced from a mantle source that shared a common and coherent depletion history. This is also evident from Fig. 8, which shows that most Site U1438 basement rocks are well correlated in Lu-Hf and Sm-Nd isochron plots. The pattern is particularly strong for the Lu-Hf system where most Site U1438 samples define a 496 Ma errorchron (Fig. 8a). In the Sm-Nd system, an errorchron through the same samples implies a somewhat younger age of 442 Ma (Fig. 8b). Assuming that measured Lu/Hf and Sm/Nd ratios of these highly depleted basalts are similar to their source (plausible for these incompatible elements), the implication is that the source of Site U1438 basalts was subject to a significant melt extraction event in the 400–500 Ma time window.

The errorchron regressions in Fig. 8 exclude two groups of outliers. The first is a group of three samples from the uppermost basement subunit 1a, which have been affected by hydrothermal alteration, as discussed by Hickey-Vargas et al. (2018). The second is a group of four samples with anomalously unradiogenic Hf and somewhat elevated Lu/Hf (Fig. 8a). The origin of the anomalously unradiogenic Hf is uncertain. Three of the samples fall within a narrow depth interval of subunit 1c at ~1525 mbsf (Fig. 3). The excursion to unradiogenic Hf in these samples is coupled to a smaller magnitude excursion in Nd isotopes (Fig. 3). The fourth sample with anomalously unradiogenic Hf is from somewhat higher in the section (subunit 1b) where the core is sparsely sampled for isotopes. For the

Table 4
Strontium isotope results for site 1438 samples.

	Depth (mbsf)	$^{87}Sr/^{86}Sr$ 6x Leached	± 2SE†	$^{87}Sr/^{86}Sr$ 3x Leached	± 2SE†	$^{87}Sr/^{86}Sr$ 1x Leached	± 2SE†
1438E61R2 3–5	1406.4	0.704265	6	0.704285	19	0.704343	29
1438E61R2 92–95	1407.3	0.704186	5				
1438E69R1 98–101	1461.9	0.704725	8	0.704710	40	0.704820	18
1438E72R1 145–148	1476.2	0.703865	4				
1438E73R2 123–128	1486.8	0.703380	7				
1438E74R2 21–24	1495.7	0.703430	6				
1438E75R1 81–85	1504.6			0.703401	6		
1438E76R2 86–91	1509.1	0.703359	7				
1438E76R3 105–110	1510.7	0.703371	5	0.703402	6		
1438E77R1 53–58	1511.4	0.703361	7	0.703383	8		
1438E77R3 41–43	1513.6			0.703477	6		
1438E78R2 127–130	1518.1			0.703476	7		
1438E78R4 49–53	1520.1	0.703562	6	0.703554	21		
1438E79R2 6–11	1525.5			0.703584	6		
1438E79R4 48–53	1528.7	0.703398	4	0.703433	7		
1438E80R2 27–30	1535.3	0.705748	4	0.705715	8	0.705765	8
1438E81R1 114–119	1544.1	0.703582	6				
1438E82R1 61–66	1552.6	0.703594	6				
1438E83R1 112–115	1562.5	0.703705	5				
1438E83R1 132–136	1562.7	0.703637	5				
1438E83R3 8–10	1564.3	0.703652	4				
1438E84R1 96–99	1572.1			0.705767	4		
1438E85R1 45–47	1579.6	0.704763	6	0.704624	16	0.704682	9
1438E85R1 124–127	1580.4			0.703614	8		
1438E86R1 25–28	1585.2						
1438E86R2 13–16	1586.4	0.703742	7				
1438E87R1 12–15	1594.1	0.703543	5	0.703573	8	0.703594	10
1438E87R1 115–118	1595.2	0.703570	9	0.703636	9		
1438E88R1 142–145	1604.5			0.703537	6		

† Uncertainties (±) reflect within-run variation calculated as 2σ standard errors (SE) and expressed as variation in the 6th decimal place.

Lu-Hf system, a regression through these samples (not shown) defines a slope that is lower than that of the main group (Fig. 8a), but for the Sm-Nd system, the implied slope is steeper (Fig. 8b). The only thing that seems clear is that that the isotopic systems of these samples have been disturbed in a way that has not affected most other Site U1438 basement rocks. As a result, the anomalous samples are excluded from further discussion of the depletion history of Site U1438 basement rocks.

If the source of Site U1438 basalts was subject to melt extraction at 400–500 Ma (as implied by the errorchrons in Fig. 8), the result should be a depletion history for the source of Site U1438 basement rocks that differs significantly than that of the depleted MORB mantle (DMM), the source of MORB. In fact, this is what is implied by the observation that trace element patterns in Site U1438 and other drill site and FAB samples are more depleted than is normally seen in MORB (Figs. 6–7), even though the long-term depletion implied by Hf and Nd isotopes is typical of MORB (Fig. 2). The point is further illustrated for the Sm-Nd system in a plot of initial Nd isotopes ($\varepsilon_{Nd\ (t)}$) versus $^{147}Sm/^{144}Nd$ (Fig. 9a) comparing Site U1438 basalts to DMM and to MORB data from Gale et al. (2013) averaged by ridge segment. It is evident that Site U1438 rocks have $^{147}Sm/^{144}Nd$ higher than most MORB and even higher than DMM of Salters and Stracke (2003). If Site U1438 basalts were derived from average DMM, they would have relatively radiogenic Nd, as seen in the highly depleted Garrett Transform basalts (Wendt et al., 1999), which include some samples with $^{147}Sm/^{144}Nd$ as high as Site U1438 basalts, but with Nd isotopes more radiogenic than DMM and Site U1438 by 3–4 epsilon units (Fig. 9a).

The offset of Site U1438 basement basalts toward high $^{147}Sm/^{144}Nd$ relative to ε_{Nd} (Fig. 9a) implies that their source was created by depletion of the chondritic reservoir (CHUR) more recently than average DMM; that is, the time of extraction from the chondritic primitive mantle (T_{CHUR} Nd) was more recent for the Site U1438 source than for the source of MORB (=DMM). Results of Nd model age calculations illustrate the point (Fig. 9b). Excluding the altered and anomalous samples identified in Fig. 8, the average Site U1438 model age is 1.45 Ga ± 0.26 (1σ), which is significantly younger than the average of 2.64 G a ± 0.65 (1σ) for Garrett Transform basalts (Fig. 9b), and the 2.2 Ga age of DMM adopted by Salters and Stracke (2003). Thus, it is clear that the source of Site U1438 basalts may be interpreted to be significantly younger than average DMM.

Alternatively, the Site U1438 source may have been a part of the DMM reservoir for much of its history if was also subject to additional and relatively recent melting

Table 5
Whole-rock trace elements for site 447 and site 1201 basement basalts.[*]

	Ti	Li	Be	Sc	V	Cr	Ni	Rb	Sr	Y	Zr	Nb	Cs	Ba	La	Ce	Pr	Nd	Sm	Eu	Gd	Tb	Dy	Ho	Er	Yb	Lu	Hf	Ta	Pb	Th	U
Site 447 Basement Basalts																																
447A 14-1[**]	6175	31.2		40.0	274	328	94	6.76	125	26.1	69.3	1.46	0.310	11.4	2.34	7.28	1.29	6.73	2.36	0.910	3.37	0.620	4.02	0.910	2.54	2.47	0.380	1.78	0.120	0.600	0.100	0.110
447A-14-2 (2–4)	6105	38.5	0.381	38.4	271	300	82	4.04	123	25.1	62.4	1.33	0.206	12.4	2.30	7.38	1.24	6.74	2.39	0.888	3.30	0.605	4.23	0.933	2.68	2.63	0.398	1.67	0.100	0.425	0.119	0.095
447A-16-2 (22–24)	5932	41.4	0.456	38.7	257	302	146	10.2	127	25.0	62.8	1.42	0.887	10.8	2.51	7.25	1.23	6.56	2.24	0.828	3.03	0.562	3.96	0.862	2.50	2.46	0.369	1.56	0.103	0.301	0.105	0.087
447A -17-2 (1–4)	7629	8.8	0.371	42.7	346	149	72	6.45	85.9	34.7	69.1	1.69	0.153	11.6	2.69	8.06	1.45	8.12	3.00	1.046	4.27	0.782	5.67	1.23	3.54	3.54	0.533	2.01	0.126	0.397	0.144	0.327
447A-17-2 (53–55)	7981	8.2	0.373	44.3	362	147	74	1.37	82.9	35.1	72.3	1.80	0.028	11.0	2.55	8.05	1.42	7.84	2.94	1.009	4.11	0.761	5.64	1.23	3.56	3.54	0.537	2.08	0.130	0.414	0.145	0.044
447A-17-3 (105–107)	7667	17.4	0.338	44.0	309	172	130	3.57	85.8	35.2	69.6	1.69	0.069	5.93	2.50	7.71	1.37	7.64	2.84	0.983	4.03	0.740	5.46	1.19	3.46	3.47	0.520	1.98	0.121	0.403	0.134	0.799
447A-17-3 (105–107) rep	7631	17.3	0.331	43.7	311	173	130	3.56	85.5	34.7	69.0	1.67	0.068	5.91	2.45	7.62	1.35	7.54	2.85	0.976	3.98	0.735	5.44	1.18	3.44	3.45	0.517	1.95	0.119	0.402	0.133	0.791
447A-21-1 (128–130)	6390	10.4	0.273	42.2	304	305	117	2.40	71.2	27.2	54.7	1.13	0.072	7.30	1.68	5.52	1.00	5.78	2.25	0.807	3.21	0.604	4.48	0.983	2.83	2.83	0.425	1.59	0.084	0.312	0.090	0.031
447A-22-1 (60–62)	6134	6.47	0.262	41.5	310	308	113	0.723	68.2	27.2	52.0	1.05	0.016	6.59	1.65	5.45	0.994	5.69	2.21	0.806	3.22	0.600	4.44	0.968	2.79	2.78	0.420	1.52	0.084	0.278	0.085	0.025
447A-23-1 (16–19)	6464	9.06	0.269	41.2	316	255	116	0.843	69.3	28.1	56.2	1.23	0.019	6.52	1.84	6.07	1.08	6.21	2.40	0.863	3.46	0.646	4.64	1.01	2.89	2.90	0.427	1.66	0.097	0.198	0.103	0.030
447A-25-1 (9–11)	4848	9.82	0.331	34.6	213	341	222	0.557	105	19.9	51.2	0.772	0.043	2.34	1.46	5.07	0.922	5.13	1.83	0.700	2.53	0.466	3.23	0.716	2.02	2.02	0.303	1.28	0.068	0.137	0.044	0.015
447A-30-2 (80–82)	5481	10.0	0.287	41.3	268	403	149	2.81	89.3	21.8	50.3	2.43	0.053	16.8	2.14	6.14	0.994	5.32	1.92	0.708	2.67	0.501	3.55	0.786	2.25	2.26	0.342	1.37	0.154	0.308	0.195	0.054
Site 1201 Basement Basalts																																
1201D-46R-3 (43–45)[***]	5156	18.3	0.300	43.3	234	368	87	15.0	490	27.5	60.0	2.02	0.350	24.3	3.23	6.54	1.16	6.00	2.03	0.750	3.17	0.600	3.96	0.910	2.64	2.72	0.440		0.134	0.560	0.139	0.201
1201D-46R-5 (6–8)[***]	5156	22.1	0.290	44.2	238	365	89	18.3	323	23.7	58.0	1.51	0.430	27.8	2.81	7.14	1.23	6.31	2.21	0.780	3.16	0.600	3.87	0.870	2.52	2.58	0.400	2.26	0.127	0.490	0.137	0.177
1201-48R-2 (92–94)	5858	11.9	0.237	41.3	268	431	130	4.13	74.8	23.0	44.4	0.628	0.077	4.31	1.30	4.70	0.883	5.25	2.08	0.695	2.91	0.557	3.97	0.865	2.41	2.45	0.369	1.35	0.054	0.302	0.045	0.163
1201D-48R-4 (66–68)	5422	12.6	0.230	40.5	252	376	125	4.16	75.4	24.5	46.8	0.631	0.071	5.09	1.36	4.78	0.902	5.33	2.12	0.793	3.08	0.570	4.09	0.903	2.57	2.53	0.386	1.39	0.053	0.436	0.051	0.175
1201D-49R-1 (11–13)	5175	11.9	0.225	39.2	249	372	132	3.19	73.4	23.1	45.2	0.594	0.083	5.50	1.27	4.47	0.851	5.04	1.98	0.763	2.91	0.541	3.84	0.843	2.41	2.40	0.358	1.33	0.055	0.283	0.048	0.094
1201D-49R-1 (47–49)	5924	14.7	0.258	42.3	271	437	138	6.98	75.3	23.2	44.4	0.648	0.141	4.73	1.34	4.81	0.874	5.16	2.06	0.689	2.87	0.551	3.92	0.853	2.40	2.42	0.370	1.37	0.055	0.519	0.047	0.054
1201D-49R-3 (37–39)	5671	14.5	0.269	42.9	267	399	109	8.10	80.8	26.0	48.5	0.650	0.188	6.31	1.49	4.71	0.908	5.29	2.09	0.784	3.01	0.563	4.06	0.899	2.58	2.56	0.389	1.40	0.053	0.256	0.047	0.157
1201D-49R-3 (37–39) rep	5644	14.4	0.272	42.5	269	398	110	8.14	80.6	26.0	48.5	0.652	0.190	6.41	1.48	4.73	0.903	5.36	2.09	0.783	3.00	0.563	4.08	0.900	2.58	2.56	0.385	1.39	0.054	0.256	0.047	0.157
1201D-51R-1 (2–4)	5327	12.7	0.235	40.2	243	375	123	4.09	86.0	23.9	46.2	0.612	0.090	7.08	1.30	4.60	0.862	5.10	2.03	0.769	2.95	0.548	3.89	0.861	2.44	2.42	0.369	1.35	0.054	0.284	0.047	0.257
1201D-52R-2 (56–58)	4901	23.5	0.223	37.7	244	352	100	3.28	70.8	21.9	43.0	0.562	0.086	8.62	1.18	4.20	0.792	4.71	1.88	0.718	2.76	0.514	3.59	0.804	2.27	2.26	0.342	1.28	0.052	0.327	0.047	0.084
1201D-53R-1 (119–121)	5374	18.6	0.247	41.3	280	368	88	5.00	73.3	24.1	46.5	0.614	0.084	5.97	1.30	4.59	0.869	5.17	2.05	0.785	3.00	0.562	4.02	0.887	2.55	2.53	0.378	1.37	0.053	0.265	0.048	0.082
1201D-65R-1 (47–49)	5273	27.8	0.250	39.6	246	355	135	2.81	74.6	23.3	46.0	0.614	0.111	5.50	1.26	4.55	0.864	5.09	2.02	0.765	2.93	0.543	3.89	0.848	2.43	2.41	0.360	1.34	0.054	0.287	0.047	0.018

[*] Units for all elements are parts-per million (ppm).
[**] Data are from Reagan et al. (2010).
[***] Data are from Savov et al. (2006).

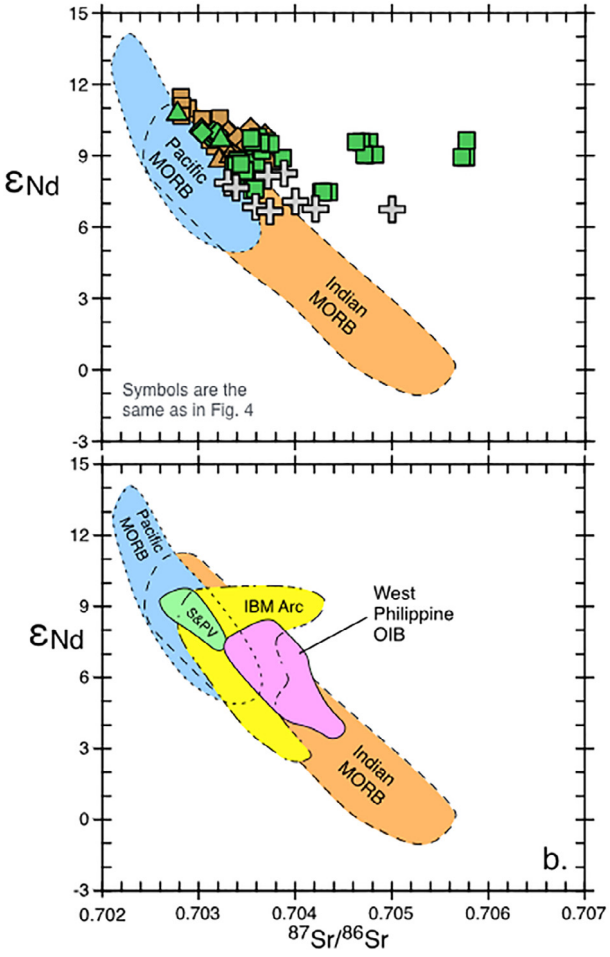

Fig. 5. Plot of ε_{Nd} versus $^{87}Sr/^{86}Sr$ comparing Site U1438 samples with Site 1201 and 447 basement basalts and with FAB, MORB, IBM arc, and West Philippine data sets. Data for Site U1438 samples are from Table 1 and 4. Other data sources are indicated in the captions to Figs. 2 and 4. The wide scatter in $^{87}Sr/^{86}Sr$ for Site U1438 basement samples at relatively constant ε_{Nd} in is interpreted to reflect effects of seawater alteration on Sr. Additional discussion of alteration effects at Site U1438 are provided by Hickey-Vargas et al. (2018).

and depletion events. The errorchron relationships in Fig. 8 provide evidence that such an event may have occurred at 400–500 Ma. The effect of such an event would be to shift $^{147}Sm/^{144}Nd$ in the mantle residue to the right in Fig. 9a, to values at least as high as observed in Site U1438 basalts. This assumes that melting at 49 Ma to create Site U1438 basalts was in the spinel field, where high-degree melting will produce basalts with parent-daughter ratios ($^{147}Sm/^{144}Nd$) that may approach (but not exceed) those of their source.

Under this scenario, the model ages (T_{CHUR} Nd values – Fig. 9b) are an average of the two events that created the distinctively depleted character of the source of site U1438 basement rocks. The first is an ancient melt extraction event at 2–3 Ga, which is associated with the creation of the DMM. The second is the melt extraction at 400–500 Ma implied by the errorchrons (Fig. 8), which drove the eventual source of Site U1438 basalts to the right in Fig. 9a, to uniquely depleted compositions with $^{147}Sm/^{144}Nd > 0.23$ and $\varepsilon_{Nd} < 10.0$. To create Site U1438 basalts, this source must have been melted again at 49 Ma at the time of IBM subduction initiation. In order for the Site U1438 basalts to inherit the trace element-depleted character of their source (e.g., $^{147}Sm/^{144}Nd > 0.23$), this must have been high-degree melting, as inferred by Hickey-Vargas et al. (2018) and by Reagan et al. (2010) for FAB.

Parkinson et al. (1998) inferred a similar depletion history for IBM forearc peridotites based on Os isotopes. Using a revised primitive mantle value for $^{187}Os/^{188}Os = 0.1292$ (Day et al., 2017), the five most depleted peridotites of Parkinson et al. (1998) give Re-depletion ages of 1.0–1.4 Ga, similar to our T_{CHUR} Nd ages for Site U1438 basalts (Fig. 9b). Parkinson et al. (1998) note that a more likely depletion history would involve melt extraction from the DMM reservoir at 500–900 Ma. This is older than our 400–500 Ma errorchron age (Fig. 8) but the calculation depends on an average $^{187}Os/^{188}Os$ value (0.1246), which is likely to be quite variable locally and across regions. For the four most depleted peridotites of Parkinson et al. (1998) a lower $^{187}Os/^{188}Os$ value for DMM (~0.122) produces model ages of 360–670 Ma which are in broad agreement with our Lu-Hf and Sm-Nd errorchron ages. The details of the choice of primitive or depleted mantle value for $^{187}Os/^{188}Os$ notwithstanding, we emphasize that both our study and the study of Parkinson et al. (1998) point to a highly depleted mantle in the eastern West Philippine Basin and IBM region, perhaps resulting from a recent (~500 Ma) melting event in the MORB source. The key effect of the two-stage depletion history is that it creates strongly depleted trace element patterns in Site U1438 basalts that have only moderately depleted Nd isotopes (Fig. 9a). The occurrence of the same depleted characteristics in basement rocks at all three west-of-KPR drill sites as well as in FAB indicates that this melting event is a regional feature of the Philippine Sea and IBM system.

Analysis of subduction-induced mixing trends for Nd isotopes and key trace element ratios also show that the highly depleted source of FAB and drill site basement basalts persists today as a component in many volcanic rocks of the modern IBM arc. This is illustrated by data patterns in ε_{Nd} vs Sm/Nd and similar plots (Fig. 10). The sub-horizontal trend of the IBM arc and rearc data reflects the mixing of fluids and melts from subducted sediment and altered oceanic crust (low Sm/Nd and variable ε_{Nd}) with a depleted mantle composition in the upper-right corner of the plot (Fig. 10). This interpretation, which is consistent with a variety of source models for IBM arc rocks (e.g., Elliott et al., 1997; Pearce et al., 1999; Tamura et al., 2005; Tollstrup et al., 2010), implies that the distinctive and highly depleted composition of the source that produced FAB and west-of-KPR basement rocks (high Sm/Nd field in Fig. 10) is present today in the IBM mantle wedge. This highly depleted source is thus regionally widespread and persistent through time in the eastern West Philippine Basin and broader IBM system. The implication is that the depleted nature of IBM FAB

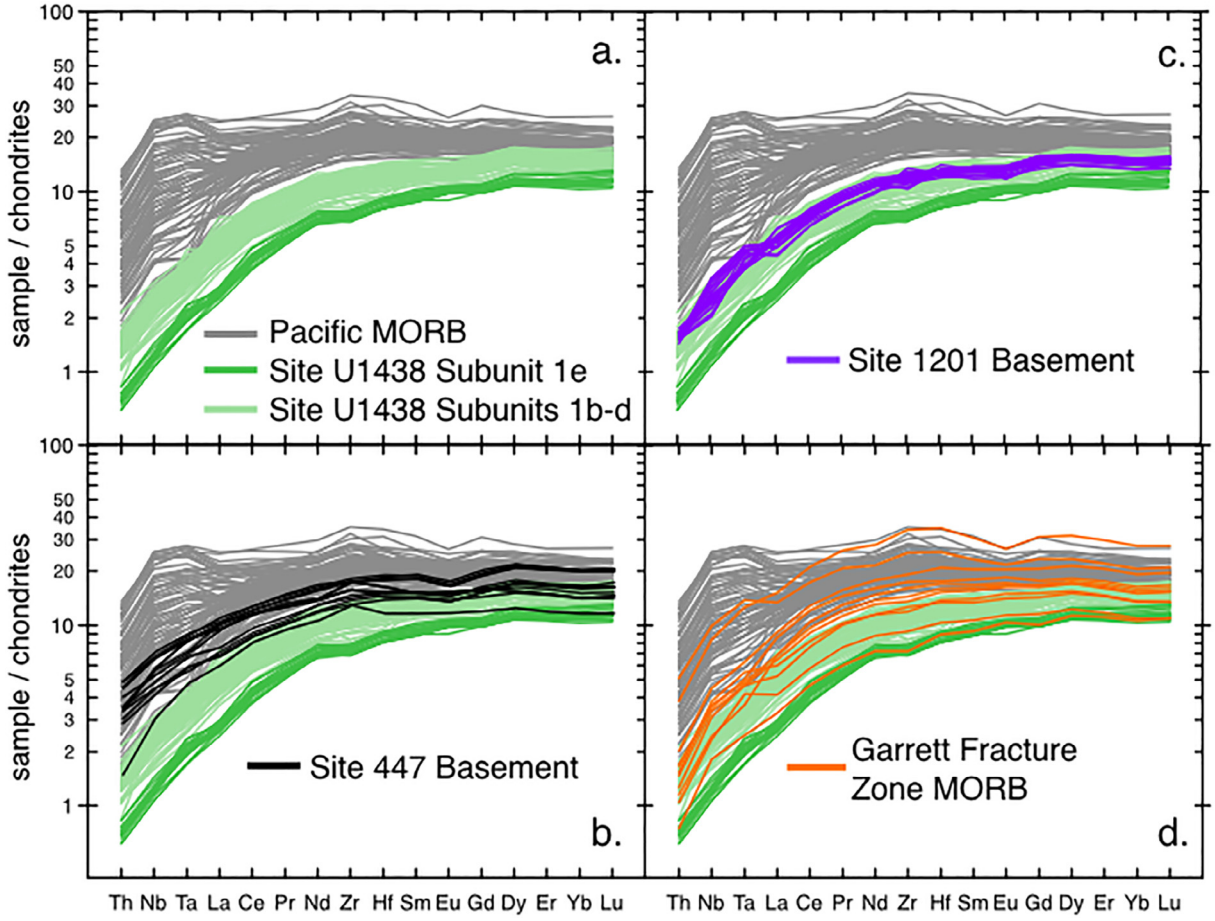

Fig. 6. Chondrite-normalized incompatible-element plots for selected immobile trace elements. This selection of elements avoids or minimizes effects of seawater alteration on Site U1438 basement basalts and other samples. High field strength (Th, Ta, Nb, Zr, Hf) and selected rare-earth element (La, Ce, Pr, Nd, Sm, Eu, Gd, Dy, Er, Yb, Lu) abundances are normalized to chondritic values of Sun and McDonough (1989). Data for Site U1438 basement samples are from Hickey-Vargas et al. (2018). Basement subunit boundaries from Hickey-Vargas et al. (2018) are shown in Fig. 3 and Table 1. Pacific MORB data from Gale et al. (2013) exclude backarc and Galapagos Spreading Center samples. Garrett Fracture Zone MORB are from Wendt et al. (1999). Data for Site 1201 and 447 basement basalts are from Table 5.

cannot be uniquely linked to melting events in the Eocene at the time of IBM subduction initiation. This point is discussed further below.

5.3. No clear evidence of subduction recycling

If basement basalts from Site U1438 and FAB from the IBM forearc sites were the first lavas to erupt at the time of subduction initiation, then it would be reasonable to anticipate that some common subduction-related geochemical effects might be expressed in both.

Effects of seawater alteration in Site U1438 samples make key elements such as K, Rb, and Ba unreliable indicators of magmatic processes and source. Subduction enrichments in Th are often correlated with Ba-enrichments in arc volcanic rocks (Kelemen et al., 2003) and the immobile nature of Th normally makes it a reliable tracer of magmatic processes in seawater-altered rocks. Excluding subunit 1a samples, which have been affected by hydrothermal alteration and metalliferous deposits at the basement-sediment contact (Fig. 12 in Hickey-Vargas et al., 2018), Site U1438 basement basalts have a mean Th/La of 0.035 (±0.004 1std dev, n = 108) and so are anomalously depleted in Th compared to normal MORB (Th/La = 0.046, Arevalo and McDonough, 2010). Site U1438 samples are also significantly more depleted than average Pacific and Indian MORB of Gale et al. (2013), which have a mean Th/La value of 0.057 (±0.027 1std dev, n = 1245). Site 447 basement basalts (mean Th/La = 0.053 ± 0.013) and FAB (mean Th/La = 0.064 ± 0.019) have Th/La that is similar to the Pacific and Indian average.

Thus, the relative abundances of Th provide no clear evidence of subduction recycling in the source of FAB or west-of-KPR drill site basement basalts. An important caveat is that this conclusion is based on whole-rock samples using only immobile element geochemistry. Our conclusions are limited in this way because nearly all available data are for whole-rock samples and because fluid-mobile element abundances have been affected by seawater alteration in most Site U1438 samples (Hickey-Vargas et al., 2018). Alteration affects in whole-rock basement samples from Site 1201 (Savov et al., 2006) and Site

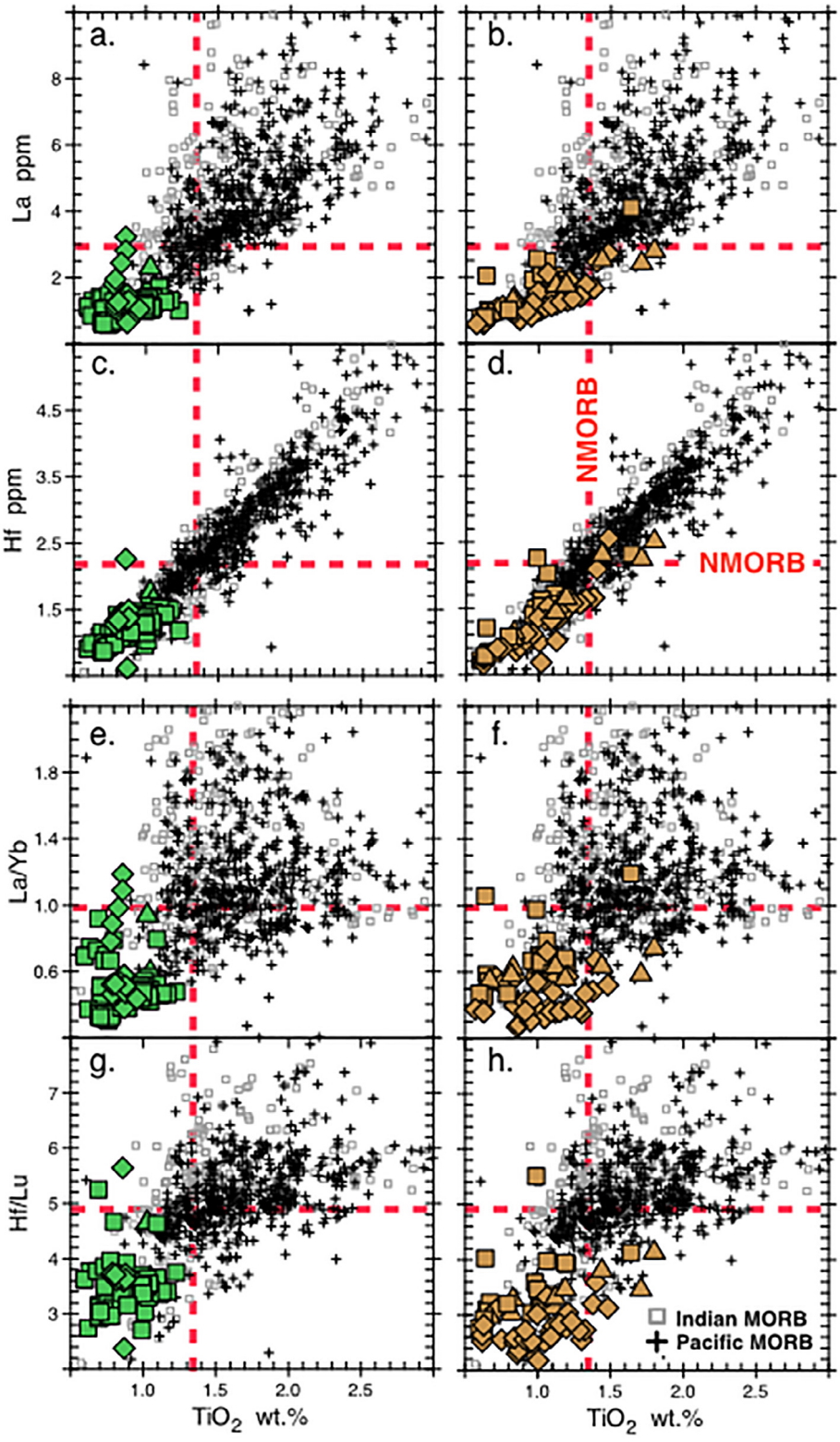

Fig. 7. Selected trace element abundances and ratios versus TiO_2 comparing drill site and FAB data with Indian and Pacific MORB. Symbols are the same as in Figs. 2 and 6. Pacific and Indian MORB data are from Gale et al. (2013). Pacific MORB excludes backarc and Galapagos Spreading Center samples. Normal MORB compositions, indicated by the red dashed line, are from Arevalo and McDonough (2010).

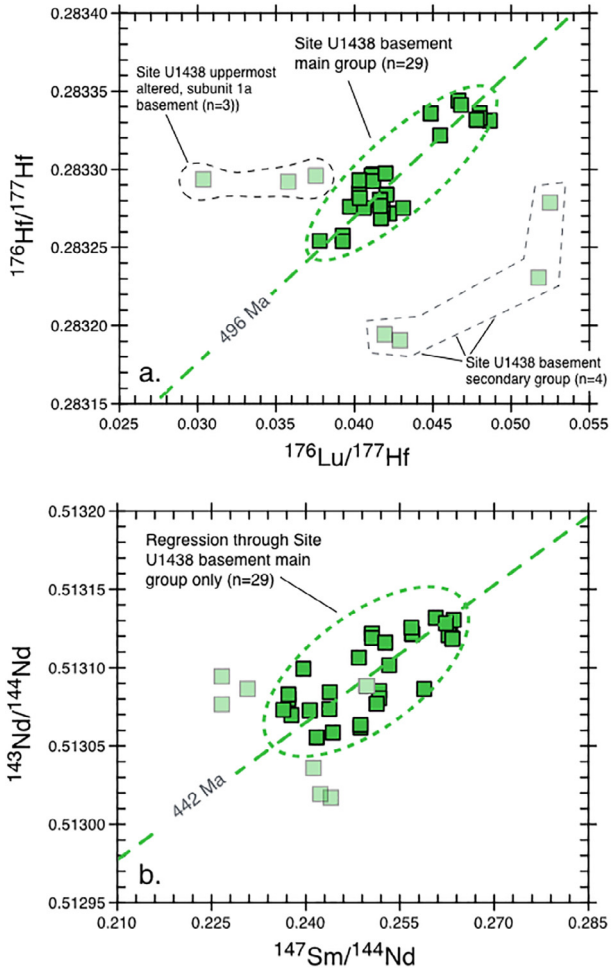

Fig. 8. Isochron plots for the Lu-Hf and Sm-Nd isotopic systems with data for Site U1438 basement rocks. Reduced major axis regressions through the main group data only (dark green symbols) define errorchrons that imply ages of ~496 Ma (^{177}Lu $\lambda = 1.867 \times 10^{-11}$) and ~442 Ma (^{147}Sm $\lambda = 6.54 \times 10^{-12}$). Samples excluded from the regressions (faded green symbols) are discussed in the text. Data are from Table 1. Values for ^{147}Sm/^{144}Nd are calculated from Sm/Nd. (For interpretation of the references to colour in this figure legend, the reader is referred to the web version of this article.)

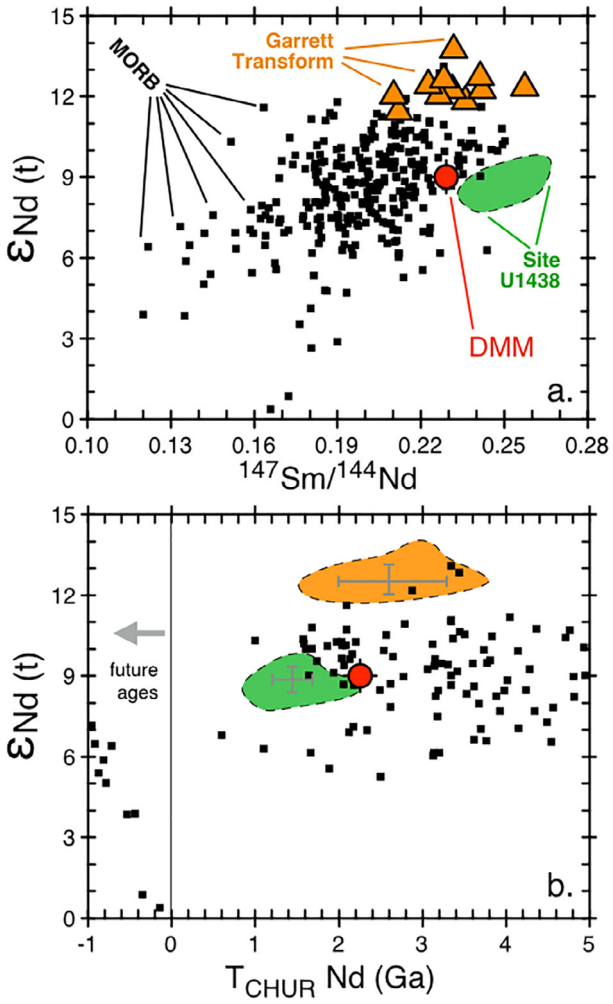

Fig. 9. Plot of initial Nd isotope compositions $\varepsilon_{Nd\ (t)}$ versus ^{147}Sm/^{144}Nd and Nd model ages (T_{CHUR} Nd) for Site U1438 basement rocks, compared to MORB, Garrett Transform basalts, and depleted MORB mantle (DMM) of Salters and Stracke (2003). Site U1438 data and DMM are corrected to 49 Ma. In panel a, Site U1438 basement rocks extend to high ^{147}Sm/^{144}Nd at lower $\varepsilon_{Nd\ (t)}$ than DMM, consistent with a younger depletion age for the Site U1438 source. This more recent depletion is shown in panel b, where the model ages of U1438 samples are significantly younger than DMM the most MORB. The gray crosses with error bars in 9b are the means ± one standard deviation for the Garret Transform and Site U1438 data. The young model ages for the Site U1438 samples can be reconciled with melting of a DMM-like source at 400–500 Ma (Fig. 8) before the melting event at 49 Ma that generated the U1438 rocks (see text for additional discussion). In panel b, only MORB and Garrett Transform samples with T_{CHUR} ages within the range of the figure are shown. Site U1438 data are from Table 1. Model ages are calculated by standard means (e.g., White, 2013) using ^{147}Sm/^{144}Nd values inferred from whole-rock Sm/Nd to determine the time elapsed since extraction from the chondritic uniform reservoir (CHUR). Values for CHUR are from Bouvier et al. (2008). MORB data are segment-averaged values from Gale et al. (2013). Garrett Transform data are from Wendt et al. (1999).

447, and for FAB also appear likely. However, recent drilling at Sites 1439–1442 (Fig. 1) has provided significant quantities of FAB and boninite glass, which appear fresh and unaffected by alteration (Pearce et al., 2014; Reagan et al., 2017). Analyses of these glasses confirm that FAB are highly depleted not only with respect to rare earth and high field strength elements, but also with respect to trace elements such as Cs, U and Rb (Reagan et al., 2016), which are normally enriched in arc volcanic rocks. Evidence of subduction recycling in Expedition 352 glasses is present only with respect to Cl and H_2O, which are significantly enriched in FAB relative to MORB (Reagan et al., 2016). The absence of traditional arc geochemical enrichments in Cs, Rb and U, the presence of excess Cl and

H_2O in these glasses compared to MORB, could indicate that FAB carry a unique and previously unrecognized fluid-enrichment signature associated with the initial stages of arc growth. The caveat in this case is that enrichments in Cl and H_2O in the absence of Cs, Rb and U might also reflect cryptic hydration of the glasses by seawater, and so yet another manifestation of seawater alteration in FAB.

5.4. Implications for FAB and the Early IBM Arc

Data presented in this paper in combination with other Expedition 351 results (Hickey-Vargas et al., 2018; Ishizuka et al., 2018) and with preliminary data from Expedition 352 (Reagan et al., 2016; Reagan et al., 2017), indicate that basement rocks just west of the KPR at Sites U1438, 1201 and 447 (Fig. 1), were very likely produced by melting of the same distinctive mantle source as FAB at and near the time of IBM subduction initiation (48–52 Ma). A key common characteristic of these rocks is the nature of their mantle source, which is highly depleted in lithophile trace elements but with Hf and Nd isotopes that are typical of Indian MORB. Model age and errorchron relationships discussed above, indicate that the depleted nature of the rocks is likely a reflection of melting events that preceded subduction initiation by hundreds of millions of years. A similar depletion history for mantle peridotites from the IBM forearc may be inferred from Re-Os isotopes (Parkinson et al., 1998). The widespread occurrence of this distinctive source throughout the region and its persistence through time in the IBM system appear inconsistent with an origin linked to subduction initiation in the Eocene. The implication is that the highly depleted nature of IBM FAB is a regional characteristic produced by ancient melting events. Consequently, such uniquely depleted basalts should not be expected in subduction-related ophiolites or other subduction initiation settings outside of the IBM system. However, if depletion-induced buoyancy of the mantle source of FAB played some dynamic roll in locating the site of IBM subduction initiation or in stabilizing the over-riding plate at the time of subduction initiation, then a general rational for finding highly depleted basalts in subduction-related ophiolites (Reagan et al., 2010) might be implied.

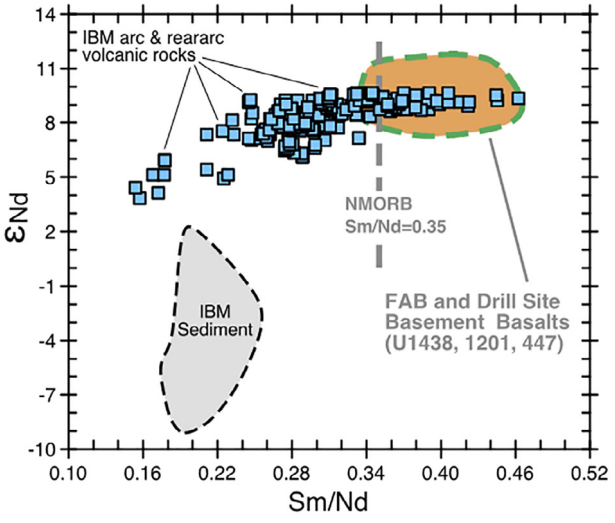

Fig. 10. Neodymium isotopes (ε_{Nd}) versus Sm/Nd comparing drill site and FAB data with modern IBM volcanic rocks and western Pacific sediment. Sediment data are from drill sites 1149, 801 and 595 from Plank and Langmuir (1998) and Vervoort and Plank (2002). Compositions of modern IBM arc and rearc volcanic rocks are from sources listed in the caption to Fig. 2 and from those listed here (Nohda and Wasserburg, 1981; Hochstaedter et al., 1990; Gill et al., 1992; Tatsumi et al., 1992; Yuasa and Nohara, 1992; Ikeda and Yuasa, 1994; Hochstaedter et al., 2001; Sun and Stern, 2001; Ishizuka et al., 2003; Tamura et al., 2005; Ishizuka et al., 2007; Ishizuka et al., 2008).

Available data indicate that west-of-KPR drill site basement rocks and FAB also lack traditional compositional signals of subduction recycling and enrichment. An important caveat for this conclusion is that a general reliance on whole-rock samples makes it difficult to distinguish subduction-related enrichments from effects of seawater alteration. We do not rule out the possibility that the drill site basement rocks and FAB may carry a unique and previously unrecognized fluid-enrichment signature associated with the initial stages of arc growth. In this context, the FAB glasses collected under Expedition 352 (Reagan et al., 2016) are likely to be a critical sample set.

ACKNOWLEDGMENTS

The authors thank E. Bair, C. Frisby and W. Buckley at the Center for Elemental Mass Spectrometry for their assistance with data collection at the University of South Carolina. Thanks also Dr. Tatiana Trejos and Dr. Jose Almirall of FIU's Trace Evidence Analysis Facility for use of the ICP mass spectrometers and for sharing their analytical expertise. The helpful support of O. Müntener and M. Chiaradia with data collection at the University of Lausanne and the University of Geneva is also gratefully acknowledged. Thanks also to S. DeBari for generously providing forearc basalt samples from 32°N and to B. Taylor for his thoughtful comments. We also extend our thanks to all members of the Exp. 351 Science Party. The hard work able assistance of the captain and entire crew of the R/V JOIDES Resolution is also gratefully acknowledged. Thanks also to V. Salters and two anonymous reviewers for their thoughtful comments, and to J. Blichert-Toft and M. Norman for their efficient handling of the manuscript.

FUNDING

This work was supported by grants from the Consortium for Ocean Leadership to co-authors who participated in Exp. 351 of the International Ocean Discovery Program (GMY, RHV, AM, IPS, OI, and RA). This work was also supported by National Science Foundation grants OCE-1537135 to GMY and MB, and OCE-1537861 to RHV; A Swiss National Science Foundation grant to O. Müntener (grant 200020/135511); a UK NERC grant (NE/M007782/1) to IPS; and a Grant-in-Aid (B) to OI (No. 25287133) for sample preparation.

APPENDIX A. SUPPLEMENTARY MATERIAL

Supplementary data associated with this article can be found, in the online version, at https://doi.org/10.1016/j.gca.2018.02.047.

REFERENCES

Abouchami W., Galer S. J. G. and Koschinsky A. (1999) Pb and Nd iotopes in NE Atlantic Fe-Mn crusts: proxies for trace metal plaeosources and paleocean circulation. *Geochim. Cosmochim.* **63**, 1489–1505.

Arculus R., Ishizuka O. and Bogus K. A. (2013) Izu-Bonin-Mariana arc origins: continental crust formation at intraoceanic arc: foundations, inceptions, and early evolution. In *IODP Scientific Prospectus* (eds. R. J. Arculus, O. Oshizuka and K. A. Bogus). https://doi.org/10.2204/iodp.sp.351.2013.

Arculus R., Ishizuka O., Bogus K., Aljahdali M. H., Bandini-Maeder A. N., Barth A. P., Brandl P. A., do Monte Guerra R., Drab L., Gurnis M. C., Hamada M., Hickey-Vargas R. L., Jiang F., Kanayama K., Kender S., Kusano Y., Li H., Loudin L. C., Maffione M., Marsaglia K. M., McCarthy A., Meffre S., Morris A., Neuhaus M., Savov I. P., Sena Da Silva C., Tepley F. J. I., van der Land C., Yogodzinski G. M. and Zhang Z. (2015a) Site U1438. In *Proceedings of the International Ocean Discovery Program* (eds. R. J. Arculus, O. Oshizuka and K. A. Bogus). https://doi.org/10.14379/iodp.proc.351.103.2015.

Arculus R., Ishizuka O., Bogus K. A., Gurnis M., Hickey-Vargas R., Aljahdali M. H., Bandini A. N., Barth A. P., Brandl P. A., Drab L., do Monte Guerra R., Hamada M., Jiang F., Kanayama K., Kender S., Kusano Y., Li H., Loudin L. C., Maffione M., Marsaglia K. M., McCarthy A., Meffre S., Morris A., Neuhaus M., Savov I. P., Sena C., Tepley F. J., van der Land C., Yogodzinski G. M. and Zhang Z. (2015b) A record of spontaneous initiation in the Izu-Bonin-Mariana arc. *Nat. Geosci.* **8**, 728–733. https://doi.org/10.1038/NGEO2515.

Arevalo, Jr, R. and McDonough W. F. (2010) Chemical variations and regional diversity observed in MORB. *Chem. Geol.* **271**, 70–85. https://doi.org/10.1016/j.chemgeo.2009.12.013.

Beguelin P., Chiaradia M., Beate B. and Spikings R. A. (2015) The Yanaurcu Volcano (Western Cordillera, Ecuador): a field, petrographic, geochemical, isotopic and geochronological study. *Lithos* **218–219**, 37–53.

Bloomer S. H. and Hawkins J. W. (1987) Petrology and geochemistry of boninite series volcanic rocks from the Mariana trench. *Contrib. Mineral.* **97**, 361–377.

Bouvier A., Vervoort J. D. and Patchett P. J. (2008) The Lu-Hf and Sm-Nd isotopic composition of CHUR: Constraints from unequilibrated chondrites and implications for the bulk composition of terrestrial planets. *Earth Planet Sci. Lett.* **273**, 48–57.

Cameron W. E., McCulloch M. T. and Walker D. A. (1983) Boninite petrogenesis: chemical and Nd-Sr isotopic constraints. *Earth Planet Sci. Lett.* **65**, 75–89.

Chiaradia M., Müntener O. and Beate B. (2011) Enriched basaltic andesites from mid-crustal fractional crystallization, recharge, and assimilation (Pilavo Volcano, Western Cordillera of Ecuador). *J. Petrol.* **52**, 1107–1141.

Day J. M. D., Walker R. J. and Warren J. M. (2017) 186Os-187Os and highly siderophile element abundance systematics of the mantle revealed by abyssal peridotites and Os-rich alloys. *Geochem. Cosmochim. Acta* **200**, 232–254.

DeBari S. M., Taylor B., Spencer K. and Fujioka K. (1999) A trapped Philippine Sea plate origin for MORB from the inner lope of the Izu-Bonin trench. *Earth Planet Sci. Lett.* **174**, 183–197.

Deschamps A. and Lallemand S. (2002) The West Philippine bain: an eocene to early Oligocene back arc basin opened between two opposed subduction zones. *J. Geophys. Res.-Sol. Ea* **107**. https://doi.org/10.1029/2001JB001706.

Elliott T., Plank T., Zindler A., White W. and Bourdon B. (1997) Element transport from slab to volcanic front at the Mariana arc. *J. Geophys. Res.-Sol. Ea* **102**, 14,991–15,019.

Gale A., Dalton C. A., Langmuir C., Su Y. and Schilling J. G. (2013) The mean composition of ocean ridge basalt. *Geochem. Geophys. Geosys.* **14**. https://doi.org/10.1029/2012GC004334.

Gill, J. B., Seales, C., Thompson, P., Hochstaedter, A. G. and Dunlap, C. (1992) Petrology and geochemistry of Pliocene-Pleistocene volcanic rocks from the Izu Arc, Leg 126, Proceedings of the Ocean Drilling Program, Scientific Results, pp. 383–404, 10.2973/odp.proc.sr.126.145.1992.

Hickey R. L. and Frey F. A. (1982) Geochemical characteristics of boninite series volcanics: implications for their source. *Geochim. Cosmochim.* **46**, 2099–2115.

Hickey-Vargas R. (1991) Isotope characteristics of submarine lavas from the Philippine Sea: implications for the origin of arc and basin magmas of the Philippine tectonic plate. *Earth Planet Sci. Lett.* **107**, 290–304.

Hickey-Vargas R. (1998) Origin of the Indian Ocean-type isotopic signature in basalts from Philippine Sea plate spreading centers: An assessment of local versus large-scale processes. *J. Geophys. Res.-Sol. Ea* **103**, 20963–20979.

Hickey-Vargas R. (2005) Basalt and tonalite from the Amami Plateau, northern West Philippine Basin: New Early Cretaceous ages and geochemical results, and their petrologic and tectonic implications. *Island Arc* **14**, 653–665.

Hickey-Vargas R., Savov I. P., Bizimis M., Ishii T. and Fujioka K. (2006) Origin of diverse geochemical signatures in igneous rocks from the Wet Philippine Basin: Implications for tectonic models. In *Back-Arc Spreading Systems: Geological, Biological, Chemical and Physical Interactions, AGU Geophysical Monograph* (ed. D. Christie), pp. 287–303.

Hickey-Vargas R., Yogodzinski G. M., Bizimis M., Ishizuka O., McCarthy A., Kusano Y., Savov I. P. and Arculus R. (2018) Origin of depleted basalts during subduction initiation: Evidence from IODP Expedition 351 Site U1438, Amami Sankaku Basin. *Geochim. Cosmochim.*.

Hilde T. W. C. and Lee C. S. (1984) Origin and evolution of the West Philippine Basin: A new interpretation. *Tectonophysics* **102**, 85–104.

Hochstaedter A. G., Gill J. B. and Morris J. D. (1990) Volcanism in the Sumisu Rift, II. Subduction and non-subduction related components. *Earth Planet Sci. Lett.* **100**, 195–209.

Hochstaedter A., Gill J. B., Peters R., Broughton P. and Holden P. (2001) Across-arc geochemical trend in the Izu-Bonin arc: contributions from the subducting slab. *Geochem. Geophys. Geosys.* **2**. https://doi.org/10.1029/2000GC000105.

Ikeda Y. and Yuasa M. (1994) Origin of alkaline volcanic rocks occurring on the volcanic front of the Izu-Mariana arc, northwest Pacific. *J. Mineral., Petrol., Econ. Geol.* **89**, 233–244. https://doi.org/10.2465/ganko.89.233.

Ishizuka O., Taylor R. N., Milton J. A. and Nesbitt R. W. (2003) Fluid-mantle interaction in an intra-oceanic arc: constraints from high-Precision Pb isotopes. *Earth Planet Sci. Lett.* **211**, 221–236. https://doi.org/10.1016/S0012-821X(03)00201-2.

Ishizuka O., Taylor R. N., Yuasa M., Milton J. A., Nesbitt R. W., Uto K. and Sakamoto I. (2007) Processes controlling along-arc isotopic variation of the southern Izu-Bonin arc. *Geochem. Geophys. Geosys.*.

Ishizuka O., Geshi N., Ito J., Kawanabe Y. and Tuzino T. (2008) The magmatic plumbing of the submarine Hachijo NW Volcanic Chain, Hachijojima, Japan: Long-distance magma transport? *J. Geophys. Res.-Sol. Ea* **B113**. https://doi.org/10.1029/2007JB005325.

Ishizuka O., Tani K., Reagan M. K., Kanayama K., Umino S., Harigane Y., Sakamoto I., Miyajima Y., Yuasa M. and Dunkley D. J. (2011) The timescales of subduction initiation and subsequent evolution of an oceanic island arc. *Earth Planet Sci. Lett.* **306**, 229–240.

Ishizuka O., Taylor R. N., Ohara Y. and Yuasa M. (2013) Upwelling, rifting, and age-progressive magmatism from the Oki-Daito mantle plume. *Geology* **41**, 1011–1014. https://doi.org/10.1130/G34525.1.

Ishizuka O., Hickey-Vargas R., Arculus R. J., Yogodzinski G. M., Kusano Y., McCarthy A., Savov I. P. and Sudo M. (2018) Age of Izu-Bonin-Mariana arc basement. *Earth Planet Sci. Lett.*.

Karig D. E. (1975) Basin genesis in the Philippine Sea. In *Initial Reports of the Deep Sea Drilling Project* (eds. J. C. Ingle, D. E. Karig and S. M. White), pp. 857–879. https://doi.org/10.2973/dsdp.proc.31.142.1975.

Kelemen P. B., Hanghøj K. and Greene A. R. (2003) One view of the geochemistry of subduction-related magmatic arcs, with an emphasis on primitive andesite and lower crust. In *Treatise on Geochemistry* (eds. H. D. Holland and K. K. Turekian). Elsevier, New York, pp. 593–659.

Kohut E., Stern R. J., Kent A. J. R., Nielsen R. L., Bloomer S. H. and Leybourne M. (2006) Evidence for adiabatic decompression melting in the Southern Mariana Arc from high-Mg lavas and melt inclusions. *Contrib. Mineral.* **152**, 201–221.

Lallemand S. (2016) Philippine Sea Plate inception, evolution, and consumption with special emphasis on the early stages of the Izu-Bonin-Mariana subduction. *Prog. Earth Planet. Sci.* **3**. https://doi.org/10.1186/s40645-016-0085-6.

Mattey D. P., Marsh N. G. and Tarney J. (1981) The geochemistry, mineralogy and petrology of basalts from the West Philippine and Parece Vela Basins and from the Palau-Kyushu and West Mariana Ridges. In *Deep Sea Dilling Project Leg 59 Initial Reports, volume 59, Washington DC* (eds. L. Kroenke and R. Scott), pp. 753–797. https://doi.org/10.2973/dsdp.proc.59.137.1981.

Meijer A. (1980) Primitive arc volcanism and a boninite series: Examples from western Pacific island arcs. In *The Tectonic and Geologic Evolution of Southeast Asian Seas and Islands, AGU Geophysical Monograph 23* (ed. D. E. Hayes). American Geophysical Union, Washington DC, pp. 269–282. https://doi.org/10.1029/GM023p0269.

Münker C., Weyer S., Scherer E. and Mezger K. (2001) Separation of high field strength elements (Nb, Ta, Zr, Hf) and Lu from rock samples for MC-ICPMS measurements. *Geochem. Geophys. Geosyst.* **2**. https://doi.org/10.1029/2001GC000183.

Nohda S. and Wasserburg G. J. (1981) Nd and Sr isotopic study of volcanic rocks from Japan. *Earth Planet Sci. Lett.* **52**, 264–276.

Ozima M., Kaneoka I., Saito K., Honda M., Yanagisawa M. and Takigami Y. (1983) Summary of geochronological studies of submarine rocks from teh western Pacific Ocean. In *Geodynamics of the Western Pacific-Indonesian Region* (eds. T. W. C. Hilde and S. Uyeda). American Geophysical Union, pp. 137–142. https://doi.org/10.1029/GD011p0137.

Parkinson I. J., Hawkesworth C. J. and Cohen A. S. (1998) Ancient mantle in a modern arc: Osmium isotopes in Izu-Bonin-Mariana forearc peridotites. *Science* **281**, 2011–2013.

Pearce J. A., van der Laan S. R., Arculus R. J., Murton B. J., Ishii T., Peate D. W. and Parkinson I. J. (1992) Boninite and harzburgite from Leg 125 (Bonin-Mariana Forearc): A case study of magmagenesis during the initial stages of subduction. *Proc. ODP, Scientific Results* **125**, 623–659.

Pearce J. A., Kempton P. D., Nowell G. M. and Noble S. R. (1999) Hf-Nd element and isotope perspective on the nature and provenance of mantle and subduction components in western Pacific arc-basin systems. *J. Petrol.* **40**, 1579–1611.

Pearce J. A., Reagan M. K., Petronotis K., Morgan S., Almeev R., Avery A. J., Carvallo C., Chapman T., Christeson G. L., Ferre E. C., Godard M., Heaton D. E., Kirchenbaur M., Kurz W., Kutterolf S., Li H., Li Y., Michibayashi K., Nelson W. R., Prytulak J., Python M., Robertson A. H. F., Ryan J. G., Sager W. W., Sakuyama T., Shervais J. W., Shimizu K. and Whattam S. A. (2014) Izu-Bonin-Mariana fore arc: Testing subduction initiation and ophiolite models by drilling the outer Izu-Bonin-Mariana fore arc, Preliminary Report, International Ocean Discovery Program Expedition 352. *International Ocean Discovery Program*. https://doi.org/10.14379/iodp.pr.352.2015.

Pin C., Briot D., Bassin C. and Poitrasson F. (1994) Concomitant separation of strontiium and samarium-neodymium for isotopic analysis in silicate samples, based on specific extraction chromatography. *Anal. Chim. Acta* **298**, 209–217.

Pin C. and Zalduegui J. F. S. (1997) Sequential separation of light rare-erth elements, thorium and uranium by miniaturized extraction chromatography: application to isotopic analyses of silicate rocks. *Anal. Chim. Acta* **339**, 79–89.

Plank T. and Langmuir C. H. (1998) The chemical composition of subducting sediment and its consequences for the crust and mantle. *Chem. Geol.* **145**, 325–394.

Reagan M. K., Ishizuka O., Stern R. J., Kelley K. A., Ohara Y., Blichert-Toft J., Bloomer S. H., Cash J., Fryer P., Hana B. B., Hickey-Vargas R., Ishii T., Kimura J. I., Peate D. W., Rowe M. C. and Woods M. (2010) Fore-arc basalts and subduction initiation in the Izu-Bonin-Mariana system. *Geochem. Geophys. Geosys.* **11**, 17. https://doi.org/10.1029/2009GC002871.

Reagan M., Brounce M., Almeev R., Shimizu K., Ryan J. G. and Pearce J. (2016). In *Volcanic glasses from Exp. 352 cores Goldschmidt Conference, Yokohama, Japan*, p. 2597.

Reagan M. K., Pearce J. A., Petronotis K., Almeev R., Avery A. J., Carvallo C., Chapman T., Christeson G. L., Ferre E. C., Godard M., Heaton D. E., Kirchenbaur M., Kurz W., Kutterolf S., Li H., Li Y., Michibayashi K., Morgan S., Nelson W. R., Prytulak J., Python M., Robertson A. H. F., Ryan J. G., Sager W. W., Sakuyama T., Shervais J. W., Shimizu K. and Whattam S. A. (2017) Subduction initiation and ophioite crust: new insights from IODP drilling. *Int. Geol. Rev.* **59**, 1439–1450. https://doi.org/10.1080/00206814.2016.1276482.

Richter C. and Ali J. R. (2015) Philippine Sea Plate motion history: Eocene-Recent record from ODP Site 1201, central West Philippine Basin. *Earth Planet Sci. Lett.*. https://doi.org/10.1016/j.epsl.2014.11.032.

Salisbury M. H., Shinohara M., Suetsugu D., Arisaka M., Diekmann B., Januszczak N. and Savov I. P. (2006) Leg 195 Synthesis: Site 1201 – A Geological and Geophysical Section in the West Philippine Basin from the 660-km Discontinuity to the Mudline. In *Proceedings of the Ocean Drilling Project, Scientific Results, Leg 195, College Station, TX (Ocean Drilling Program)* (eds. M. Shinohara, M. H. Salisbury and C. Richter), pp. 1–27. https://doi.org/10.2973/odp.proc.sr.195.113.2006.

Salters V. J. M. and Stracke A. (2003) Composition of the depleted mantle. *Geochem. Geophys. Geosyst.* **5**. https://doi.org/10.1029/2003GC000597.

Savov I. P., Hickey-Vargas R., D'Antonio M., Ryan J. G. and Spadea P. (2006) Petrology and geochemistry of West Philippine Basin Basalts and early Palau-Kyushu Arc volcanic clasts from ODP Leg 195, Site 1201D: implications for the early history of the Izu–Bonin–Mariana Arc. *J. Petrol.* **47**, 277–299.

Shipboard_Scientific_Party (1981) Site 447: East Side of the West Philippine Basin. In *Deep Sea Dilling Project Leg 59 Initial Reports, volume 59, Washington DC* (eds. L. Kroenke and R. Scott), pp. 21–110. https://doi.org/10.2973/dsdp.proc.59.102.1981.

Stern R. J. and Bloomer S. H. (1992) Subduction zonei nfancy: Examples from the Eocene Izu-Bonin-Mariana and Jurassic California arcs. *Geol. Soc. Am. Bull.* **104**, 1621–1636.

Stern R. J., Kohut E., Bloomer S. H., Leybourne M., Fouch M. and Vervoort J. D. (2006) Subduction factory processes beneath the Guguan cross-chain, Mariana Arc: no role for sediments, are serpentinites important? *Contrib. Mineral.* **151**, 202–221.

Sun S. S. and McDonough W. F. (1989) Chemical and isotopic systematics of oceanic basalts: implications for mantle composition and processes. In *Magmatism in the Ocean Basins* (eds. A. D. Saunders and M. J. Norry). Blackwell Scientific Publications, Oxford, pp. 313–346.

Sun C. H. and Stern R. J. (2001) Genesis of Mariana shoshonites: Contributions of the subduction component. *J. Geophys. Res.-Sol. Ea* **B106**, 589–608. https://doi.org/10.1029/2000JB900342.

Tamura Y., Tani K., Ishizuka O., Chang Q., Shukuno H. and Fiske R. S. (2005) Are arc basalts dry, wet, or both? Evidence from the Sumisu Caldera Volcano, Izu-Bonin Arc, Japan. *J. Petrol.* **46**, 1769–1803.

Tamura Y., Gill J. B., Tollstrup D., Kawabata H., Shkuno H., Chang Q., Miyazaki T., Takahashi N., Hirahara Y., Kodaira S., Ishizuka O., Suzuki T., Kido Y., Fiske R. S. and Tatsumi Y. (2009) Silicic magmas in the Izu-Bonin oceanic arc and implications for crustal evolution. *J. Petrol.* **50**, 685–723. https://doi.org/10.1093/petrology/egp017.

Tamura Y., Ishizuaka O., Stern R. J., Shukuno H., Kawabata H., Embley R. W., Hirahara Y., Chang Q., Kimura J. I., Tatsumi Y., Nunokawa A. and Bloomer S. H. (2011) Two primary basalt magma types from Northwest Rota-1 Volcano, Mariana Arc and its mantle diapir or mantle wedge plume. *J. Petrol.* **52**, 1143–1183. https://doi.org/10.1093/petrology/egr022.

Tatsumi Y., Murasakia M. and Nohda S. (1992) Across-arc variation of lava chemistry in the Izu-Bonin arc: identification of subuction components. *J. Volcanol. Geoth. Res.* **49**, 179–190.

Todt W., Clift R. A., Hanser A. and Hofmann A. W. (1996) Evaluation of a 202Pb-205Pb double spike for high precision lead analysis. In *Earth Processes: Reading the Isotopic Code: Geophysical Monograph 95* (eds. A. Basu and S. R. Hart). Am. Geophys Union, Washington, DC, pp. 429–437.

Tollstrup D., Gill J. B., Prinkey D., Williams R., Tamura Y. and Ishizuka O. (2010) Across-arc geochemical trends in the Izu-Bonin arc: Contributions from the subducting slab, revisited. *Geochem. Geophys. Geosys.* **11**, 27. https://doi.org/10.1029/2009GC002847.

Vervoort J. D. and Blichert-Toft J. (1999) Evolution of the depleted mantle; Hf isotope evidence from juvenile rocks through time. *Geochim. Cosmochim.* **63**, 533–556.

Vervoort J. D. and Plank T. (2002) *The Hf-Nd isotopic fingerprint of subducting sediments - a tale of two trenches*. Eos. Trans. AGU, p. 83.

Wade J. A., Plank T., Stern R. J., Tollstrup D. L., Gill J. B., O'Leary J. C., Eiler J. M., Moore R. B., Woodhead J. D., Trusdell F., Fischer T. P. and Hilton D. R. (2005) The May 2003 eruption of Anatahan volcano, Mariana Islands: Geochemical evolution of a silicic island-arc volcano. *J. Volcanol. Geoth. Res.* **146**, 139–170.

Weis D., Maerschalk C., Barling J., Williams G. A., Hanano D., Pretorius W., Mattielli N., Scoates J. S., Goolaerts A., Friedman R. M. and Mahoney J. B. (2006) High-precision isotopic characterization of USGS reference materials by TIMS and MC-ICP-MS. *Geochem. Geophys. Geosys.* **7**. https://doi.org/10.1029/2006GC001283.

Weis D., Kieffer B., Hanano D., Silva I. N., Barling J. and Pretorius W. (2007) Hf isotope compositions of U.S. Geological Survey reference materials. *Geochem. Geophys. Geosys.* **8**. https://doi.org/10.1029/2006GC001473.

Wendt J. I., Regelous M., Niu Y., Hekinian R. and Collerson K. D. (1999) Geochemistry of lavas from the Garrett Transform Fault: insights into mantle heterogeneity beneath the eastern Pacific. *Earth Planet Sci. Lett.* **173**, 271–284.

Westerhold T., Röhl U., Frederichs T., Bohaty S. M. and Zachos J. C. (2015) Astronomical calibration of the geological timescale: closing the middle Eocene gap. *Clim. Past* **11**, 1181–1195. https://doi.org/10.5194/cp-11-1181-2015.

White W. M. (2013) *Geochemistry*. John Wiley & Sons Ltd. Publishing, Oxford, UK.

White W. M., Albarède F. and Télouk P. (2000) High-precision analysis of Pb isotope ratios using multi-collector ICP-MS. *Chem. Geol.* **167**, 257–270.

White W. M. and Patchett J. (1984) Hf-Nd-Sr isotopes and incompatible element abundances in island arcs: implications for magma origins and crust-mantle evolution. *Earth Planet Sci. Lett.* **67**, 167–185.

Woodhead J., Hergt J., Davidson J. P. and Eggins S. M. (2001) Hafnium isotope evidence for 'conservative' element mobility during subduction zone processes. *Earth Planet Sci. Lett.* **192**, 331–346.

Woodhead J., Stern R. J., Pearce J. A., Hergt J. and Vervoort J. D. (2012) Hf-Nd isotope variation in Mariana Trough basalts: The importance of "ambient mantle" in the interpretation of subduction zone magmas. *Geology* **40**, 539–542. https://doi.org/10.1130/G32963.1.

Woodhead J. D. (1989) Geochemistry of the Mariana arc (western Pacific): Source composition and processes. *Chem. Geol.* **76**, 1–24.

Yogodzinski G. M., Brown S. T., Kelemen P. B., Vervoort J. D., Portnyagin M., Sims K. W. W., Hoernle K., Jicha B. and Werner R. (2015) The role of subducted basalt in the source of island arc magmas: evidence from seafloor lavas of the western Aleutians. *J. Petrol.* **56**, 441–492. https://doi.org/10.1093/petrology/egv006.

Yuasa M. and Nohara M. (1992) Petrographic and geochemical along-arc variations of volcanic rocks on the volcanic fron of the Izu-Ogasawara (Bonin) Arc. *Bull. Geol. Survey Jpn.* **43**, 421–456.

Zakariadze G. S., Dmitriev L. V., Sobolev A. V. and Suschevskaya N. M. (1981) Petrology of Basalts of Holes 447A, 449, and 450, South Philippine Sea Transect, Deep Sea Drilling Project Leg 59. In *Deep Sea Dilling Project Leg 59 Initial Reports, volume 59, Washington DC* (eds. L. Kroenke and R. Scott), pp. 669–680. https://doi.org/10.2973/dsdp.proc.59.129.1981.

Associate editor: Janne Blichert-Toft